Experimental Measurements and Kinetic Modeling of CH_4/O_2 and $CH_4/C_2H_6/O_2$ Conversion at High Pressure

CHRISTIAN LUND RASMUSSEN, JON GEEST JAKOBSEN, PETER GLARBORG

Department of Chemical and Biochemical Engineering, Technical University of Denmark, DK-2800 Kgs. Lyngby, Denmark

Received 27 September 2007; revised 5 February 2008, 24 April 2008; accepted 2 May 2008

DOI 10.1002/kin.20352
Published online in Wiley InterScience (www.interscience.wiley.com).

ABSTRACT: A detailed chemical kinetic model for homogeneous combustion of the light hydrocarbon fuels CH_4 and C_2H_6 in the intermediate temperature range roughly 500–1100 K, and pressures up to 100 bar has been developed and validated experimentally. Rate constants have been obtained from critical evaluation of data for individual elementary reactions reported in the literature with particular emphasis on the conditions relevant to the present work. The experiments, involving CH_4/O_2 and $CH_4/C_2H_6/O_2$ mixtures diluted in N_2, have been carried out in a high-pressure flow reactor at 600–900 K, 50–100 bar, and reaction stoichiometries ranging from very lean to fuel-rich conditions. Model predictions are generally satisfactory. The governing reaction mechanisms are outlined based on calculations with the kinetic model. Finally, the mechanism was extended with a number of reactions important at high temperature and tested against data from shock tubes, laminar flames, and flow reactors. © 2008 Wiley Periodicals, Inc. Int J Chem Kinet 40: 778–807, 2008

INTRODUCTION

Methane is probably the most frequently studied hydrocarbon fuel, partly because it is the simplest hydrocarbon and partly because it is the main component in natural gas. The dominating mechanism for methane oxidation depends strongly on the temperature and pressure regime. Both the high-temperature conversion important in combustion processes and the low-temperature chemistry relevant for direct conversion of methane to higher value products have received considerable attention. Oxidation of methane has been studied in static reactors [1–3], laboratory flow reactors [4–12], shock tubes [13–25], and laminar premixed flames [26–42]. However, experimental data obtained at high pressures are scarce. Shock tube studies have yielded results at pressures up to 480 bar at high temperatures [20,23,24], and results

The work is part of the CHEC (Combustion and Harmful Emission Control) research program.

Correspondence to: Peter Glarborg; e-mail: pgl@kt.dtu.dk.

Contract grant sponsor: Technical University of Denmark.
Contract grant sponsor: Danish Technical Research Council.

"Experimental Measurements and Kinetic Modeling of CH_4/O_2 and $CH_4/C_2H_6/O_2$ Conversion at High Pressure" and "Master mechanism C/H/O/N" are available as supporting information in the online issue at www.interscience.wiley.com.

at intermediate temperatures and high pressure are available from static reactor experiments (660–870 K, 1–1100 bar) [3]. Combustion-related flow reactor studies, e.g. [7,12], are often limited to pressures below 20 bar, whereas studies of homogeneous partial oxidation of CH_4 to CH_3OH [43–52] typically operate in the 20–100 bar and 600–900 K range, similar to the present study but limited to very reducing conditions. Finally, data are available on oxidation of CH_4 in supercritical water (663–923 K, 35–350 bar) [53–58].

The objective of the present work is to develop and validate a detailed chemical kinetic model for homogeneous combustion of CH_4/natural gas in the intermediate temperature range (600–900 K) and high pressure (50–100 bar). Instead of relying on a previous kinetic model, the reaction mechanism is developed from a critical review of available rate constants from the literature. The model is validated through comparison with experimental results from diluted systems of CH_4/O_2 and $CH_4/C_2H_6/O_2$ obtained under well-defined conditions in a high-pressure laminar flow reactor at stoichiometries ranging from highly lean to fuel-rich conditions.

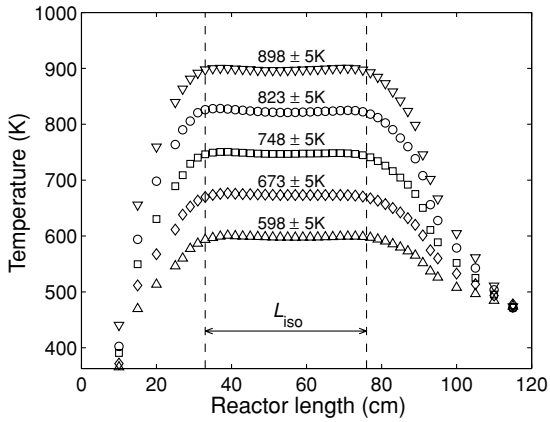

Figure 1 Measured temperature profiles across the reaction zone. The vertical dashed lines delimit the isothermal section of the reactor: $L_{iso} = 43$ cm.

EXPERIMENTAL

The experimental work has been conducted in a laboratory-scale high-pressure laminar flow reactor designed to approximate plug flow. The setup is described in detail elsewhere [59], and only a brief description is provided here. The system enables well-defined investigations of homogeneous gas-phase chemistry at pressures from 10 to 100 bar, temperatures up to 925 K, and flow rates of 1–5 L/min (STP). The reactions take place in a tubular quartz reactor, enclosed in a stainless steel tube that acts as a pressure shell. The steel tube is placed in a tube oven with three individually controlled electrical heating elements that produce an isothermal reaction zone (±5 K) of 43 cm. This is verified by the measured temperature profiles shown in Fig. 1. The reactor temperature is monitored by type K thermocouples (±2.2 K or 0.75%) positioned in the void between the quartz reactor and the steel shell.

The reactant gases are premixed before entering the reactor. All gases used in the experiments are high purity gases or mixtures with certificated concentrations (±2% uncertainty). The system is pressurized from the feed gas cylinders. Downstream of the reactor, the system pressure is reduced to atmospheric level prior to product analysis, which is conducted by an online 6890N Agilent gas chromatograph (GC-TCD/FID from Agilent Technologies). The GC has three operational columns (DB1, Porapak N, and Molesieve 13×) and uses flame ionization (hydrocarbons) and thermal conductivity (other species) for detection. With helium as carrier gas, the GC is used for detection of CH_4, O_2, CO, CO_2, CH_3OH, and CH_3NO_2 with an overall relative measuring uncertainty in the range ±2–6%, while the current configuration does not allow a sufficiently accurate determination of H_2. Attempts to detect CH_2O were not successful, possibly due a loss mechanism downstream of the reactor. In the figure captions, the uncertainties for the individual species are listed for each experiment, based on a first-order uncertainty analysis, taking into consideration the uncertainties associated with calibration gases, flows, analyzers, etc.

Experimental data are obtained as mole fractions as a function of the reactor temperature measured at intervals of 25 K. All experiments are conducted in mixtures highly diluted in N_2, which ensures a low heat development during the reaction. The reactor operates in the laminar flow regime under conditions that approximate plug flow. It is reasonable to approximate the laminar flow field to plug flow and reduce the mathematical description from a 2D to a 1D problem if the gas is premixed and the radial velocity gradients are sufficiently small to allow fluid elements to exhibit similar residence times. On the basis of the correlations by Levenspiel [60,61], we showed in a previous paper [59] that conditions with low axial dispersion are obtained at volumetric flow rates of 1–3 L/min (STP), whereas at the highest flow rate (5 L/min) the plug flow assumption is questionable. In the present work, all experiments have been conducted with a volumetric flow rate of 3 L/min under which conditions, it is still reasonable to assume plug flow.

DETAILED KINETIC MODEL

The proposed reaction mechanism includes subsets for H_2/O_2 and CO/CO_2 drawn from a preceding paper [59]. These subsets are supplemented by elementary reactions with C_1 and C_2 hydrocarbons. Part of the hydrocarbon subset is adopted from recent work on CH_3OH oxidation [62]. The most important reactions are discussed below, with special attention to pressure-dependent reactions.

Thermodynamic Properties

Table I lists the thermodynamic properties for hydrocarbon species considered in the current model. With a few exceptions, data are drawn from the Thermochemical Database of Burcat and Ruscic [63] and include evaluations from the Active Thermochemical Tables of Ruscic and coworkers [64,65].

In the literature, thermodynamic properties of alkylperoxide species and their radical derivatives often vary considerably. In the present work, the species CH_3OOH, CH_3OO, CH_2OOH, C_2H_5OOH, and C_2H_5OO warrant a few supplementary comments. The preferred value of $\Delta_f H_{298}(CH_3OOH) = -30.1 \pm 1$ kcal/mol is obtained from the recent experimental work by Matthews et al. [66], which is supported by theoretical values [66,67]. For $\Delta_f H_{298}(CH_3OO)$ we prefer the theoretical value of 3.4 kcal/mol from Janoschek and Rossi [68], in reasonable agreement with recent experimental values of 2.1 ± 1.2 kcal/mol [69], 4.8 ± 1.2 kcal/mol [67], and 3.0 ± 1.2 kcal/mol [70]. Enthalpies of formation of C_2H_5OOH and C_2H_5OO are both drawn from the work of Blanksby et al. [67], which within uncertainty limits is in agreement with a range of studies [69,71–73].

C_1 Hydrocarbon Subset

The proposed C_1 hydrocarbon subset is presented in Table II. The mechanism only includes elementary reactions for compounds relevant to the investigated conditions. Reaction pathways leading to, e.g., methylene (CH_2) and methylidyne (CH) from saturated hydrocarbon fuels are typically very endothermic and unimportant in the temperature range of interest. To extend the application of the present mechanism to combustion systems operated at higher temperatures, relevant subsets of these species must be included from relevant sources. This is discussed in the appendix, where the kinetic model is extended and tested against a wider range of experimental data.

Methane is converted through a number of H-abstraction reactions, most importantly the radical reactions with H (R1), O (R2), OH (R3), and HO_2 (R4), but also the initiation reaction with molecular oxygen (–R13). For (R1) and (R3), we have adopted the rate constants from recent work of Michael and coworkers [74,75], who combined shock tube measurements with a literature review to provide rate expressions valid over a wide temperature range. At higher temperatures, both values are about 20% below the evaluation by Baulch et al. [76]. For (R2) and (R4), we follow the Baulch recommendation; like (R1) and (R3), (R2) is well characterized at medium to high temperatures, whereas measurements of (R4) is limited to a single relative rate measurement of $k_4/k_{HO_2+HO_2}^{1/2}$ at 716 K [77]. For the initiation reaction CH_4+O_2 (–R13), we rely on the theoretical work of Zhu and Lin [78], which is supported by flow reactor results at 1000 K [79] and recent shock tube data [80], but a factor of 1.5–2.5 higher than the estimated value of Baulch et al. [76]. Reactions with hydrocarbon radicals, e.g., CH_3O (R51) and HCO (–R84), gain importance under reducing conditions, whereas reactions involving peroxy radicals, e.g. HO_2 (R4) and CH_3OO (R23), constitute conversion channels at high pressure and/or low temperatures.

The most important reaction of CH_3 is that with molecular oxygen (R9, R10, R11). The association channel to CH_3OO (R9) dominates at high pressure and/or low and intermediate temperatures (<1000 K), whereas (R10) and (R11) become competitive at higher temperatures. The recent work by Fernandes et al. [81] on (R9) characterized the temperature and pressure dependency from measurements in the range 1–1000 bar and 300–700 K. Since their representation of the Troe formalism is not directly compatible with the CHEMKIN-II software package [82], we have refitted the rate constant at specific pressures (Table II). The rate constants for (R10) and (R11) are adopted from the recent shock tube study by Srinivasan et al. [83], who combined their own measurements with literature data [84–86] across the temperature range 1237–2430 K.

Since methyl has a low reactivity, reactions with other radicals may become important. The reaction of CH_3 with HO_2 offers a direct oxidation path to CH_3O (R12), or regeneration of CH_4 (R13). The increased availability of HO_2 at high pressure brings (R12) in competition with reaction of CH_3 with O_2 (R9). Only a few experimental values of k_{12} have been reported [79,87,88], and they all rely on indirect determinations. The recombination of CH_3 with atomic hydrogen (R5) is well characterized over a wide range of temperature, pressure, and bath gases [89]; however, data on the collision efficiency of N_2 are scarce. Even though the recombination of CH_3 radicals to C_2H_6 (R14) is well established over a large temperature and pressure range [76], some uncertainty remains in the temperature

Table I Thermodynamic Properties of Species Included in the Reaction Mechanism

Name	Formula	H_{298}	S_{298}	$C_{p,400}$	$C_{p,600}$	$C_{p,800}$	$C_{p,1000}$	$C_{p,1500}$	T-range	Ref.
Methyl radical	CH_3	35.01	46.36	9.98	11.50	12.86	14.09	16.25	200–6000	[63]
Methane	CH_4	−17.83	44.52	9.65	12.48	15.04	17.16	20.58	200–6000	[63]
Hydroxymethyl radical	CH_2OH	−4.11	58.35	12.79	15.36	17.08	18.44	20.59	200–6000	[63]
Methoxy radical	CH_3O	4.84	55.98	12.05	15.47	17.86	19.70	22.25	200–6000	[63]
Methanol	CH_3OH	−48.04	57.51	12.07	15.98	19.00	21.38	25.07	200–6000	[63]
Methylperoxyl radical	CH_3OO	3.00	64.44	15.05	19.17	22.05	24.20	27.31	200–6000	[63,70]
Hydroperoxymethyl radical	CH_2OOH	15.79	65.89	17.16	21.28	24.16	26.31	29.42	200–2500	[204][a]
Methylperoxide	CH_3OOH	−30.10	65.94	18.83	23.02	25.52	27.50	30.65	200–6000	[63,66]
Formaldehyde	CH_2O	−25.95	52.28	9.36	11.52	13.37	14.82	16.93	200–6000	[63]
Formyl radical	HCO	10.11	53.59	8.75	9.84	10.85	11.66	12.94	200–6000	[63]
Acetylene	C_2H_2	54.52	48.01	12.01	13.89	15.16	16.23	18.14	200–6000	[63]
Vinyl radical	C_2H_3	70.88	55.84	11.81	14.90	17.06	18.78	21.50	200–6000	[63]
Ethylene	C_2H_4	12.54	52.41	12.58	16.95	20.05	22.49	26.19	200–6000	[63]
Ethyl radical	C_2H_5	28.36	59.05	14.59	19.35	22.93	25.78	30.16	200–6000	[63]
Ethane	C_2H_6	−20.04	54.77	15.57	21.36	25.80	29.32	34.71	200–6000	[63]
Ketene	CH_2CO	−11.40	57.80	14.20	16.89	18.79	20.25	22.48	200–6000	[63]
Acetyl radical	CH_3CO	−2.46	63.91	14.27	18.13	20.99	23.19	26.34	200–6000	[63]
Formylmethyl radical	CH_2CHO	6.00	64.02	15.15	18.60	21.30	23.34	26.35	300–5000	[63]
Acetaldehyde	CH_3CHO	−39.79	63.07	15.78	20.58	24.16	26.91	30.96	200–6000	[63]
Ethanol	C_2H_5OH	−56.15	67.05	19.31	25.96	30.59	34.15	39.53	200–6000	[63]
1-Hydroxyethyl radical	1-C_2H_4OH	−12.91	69.06	18.30	23.48	27.16	30.02	34.52	200–6000	[63]
2-Hydroxyethyl radical	2-C_2H_4OH	−5.70	69.70	19.38	24.40	27.94	30.70	35.00	200–6000	[63]
Hydroxyethylperoxyl radical	$HOC_2H_4O_2$	−38.60	84.71	24.77	30.25	34.42	37.74	41.73	300–2500	[143]
Ethoxy radical	C_2H_5O	−3.25	66.34	18.93	24.34	28.35	31.44	36.01	200–6000	[63]
Ethylperoxyl radical	C_2H_5OO	−6.80	71.69	21.52	28.48	33.41	37.06	42.30	200–6000	[63,67]
Ethylperoxide	C_2H_5OOH	−39.50	75.17	24.29	31.70	36.63	40.19	45.28	200–6000	[63,67]
1-Hydroperoxyethyl radical	CH_3CHOOH	6.43	74.84	23.60	30.57	35.50	39.15	44.39	200–2500	[204][b]
Vinyloxy radical	CH_2CHO	3.05	61.85	15.04	19.14	21.93	24.02	27.13	200–6000	[63]
Ethenol	H_2CCHOH	−29.80	69.30	17.72	22.86	26.31	28.91	32.82	200–6000	[63]

Units are kcal/mol for H, and cal/(mol K) for S and C_p. Temperature (T) range is in K.

[a] $C_{p,298} = 14.89$ cal/(mol K) obtained from Janoschek and Rossi [204]. $C_p(T)$ is fitted to this value with the temperature dependence adopted from $C_p(T)(CH_3OO)$ [63].

[b] $C_{p,298} = 19.70$ cal/(mol K) obtained from Janoschek and Rossi [204]. $C_p(T)$ is fitted to this value with the temperature dependence adopted from $C_p(T)(C_2H_5OO)$ [63].

Table II Reactions from the C_1 Hydrocarbon Reaction Mechanism

	Reactions	A	β	E	Note/Ref.
1.	$CH_4 + H \rightleftharpoons CH_3 + H_2$	4.10×10^3	3.156	8,755	[74]
2.	$CH_4 + O \rightleftharpoons CH_3 + OH$	4.40×10^5	2.5	6,580	[76]
3.	$CH_4 + OH \rightleftharpoons CH_3 + H_2O$	1.00×10^6	2.182	2,506	[75]
4.	$CH_4 + HO_2 \rightleftharpoons CH_3 + H_2O_2$	4.70×10^4	2.5	21,000	[76]
5.	$CH_3 + H(+M) \rightleftharpoons CH_4(+M^a)$	2.11×10^{14}	0.0	0	[89]
	Low-pressure limit:	6.47×10^{23}	−1.8	0	
	Troe parameters: 0.638 10^{-30} 3230 10^{30}				
6.	$CH_3 + O \rightleftharpoons CH_2O + H$	6.91×10^{13}	0.0	0	[76,100]
7.	$CH_3 + O \rightleftharpoons H_2 + CO + H$	1.52×10^{13}	0.0	0	[76,100]
8.	$CH_3 + OH(+M) \rightleftharpoons CH_3OH(+M)$	4.34×10^{15}	−0.79	0	[101]
	Low-pressure limit:	3.84×10^{37}	−6.21	1,333	
	Troe parameters: 0.25 210 1434 10^{30}				[b]
[c]9.	$CH_3 + O_2 \rightleftharpoons CH_3OO$	5.00×10^{22}	−3.85	2,000	1 bar, [81][d]
	$CH_3 + O_2 \rightleftharpoons CH_3OO$	3.35×10^{21}	−3.2	2,300	10 bar
	$CH_3 + O_2 \rightleftharpoons CH_3OO$	4.10×10^{20}	−2.94	1,900	20 bar
		3.25×10^{29}	−5.6	6,850	[20 bar
	$CH_3 + O_2 \rightleftharpoons CH_3OO$	2.83×10^{18}	−2.2	1,400	50 bar
		5.60×10^{28}	−5.25	6,850	50 bar
	$CH_3 + O_2 \rightleftharpoons CH_3OO$	1.05×10^{19}	−2.3	1,800	100 bar
		4.10×10^{30}	−5.7	8,750	100 bar
10.	$CH_3 + O_2 \rightleftharpoons CH_3O + O$	7.55×10^{12}	0.0	28,297	[83]
11.	$CH_3 + O_2 \rightleftharpoons CH_2O + OH$	1.87×10^{11}	0.0	9,842	[83]
12.	$CH_3 + HO_2 \rightleftharpoons CH_3O + OH$	2.00×10^{13}	0.0	1,075	[88]
13.	$CH_3 + HO_2 \rightleftharpoons CH_4 + O_2$	2.55×10^8	1.25	−1,645	[78], 300–800 K
		1.82×10^3	2.83	−3,730	800–3000 K
14.	$CH_3 + CH_3(+M) \rightleftharpoons C_2H_6(+M)$	3.60×10^{13}	0.0	0	[76]
	Low-pressure limit:	1.27×10^{41}	−7.0	2,760	
	Troe parameters: 0.62 73 1180 10^{30}				
15.	$CH_3 + CH_3 \rightleftharpoons C_2H_5 + H$	5.42×10^{13}	0.0	16,055	[76]
16.	$CH_3OO + H \rightleftharpoons CH_3O + OH$	9.64×10^{13}	0.0	0	[106]
17.	$CH_3OO + O \rightleftharpoons CH_3O + O_2$	1.63×10^{13}	0.0	−445	($=k_{HO_2+O}$ [76])
18.	$CH_3OO + OH \rightleftharpoons CH_3OH + O_2$	2.00×10^{15}	−0.60	0	see text
19.	$CH_3OO + OH \rightleftharpoons CH_3O + HO_2$	4.00×10^{11}	0.60	0	see text
20.	$CH_3OO + HO_2 \rightleftharpoons CH_3OOH + O_2$	2.50×10^{11}	0.0	−1,490	[108]
21.	$CH_3OO + CO \rightleftharpoons CH_3O + CO_2$	1.57×10^5	2.18	17,940	($=k_{CO+HO_2}$ [205])
22.	$CH_3OO + CH_3 \rightleftharpoons CH_3O + CH_3O$	5.06×10^{12}	0.0	−1,410	[113]
23.	$CH_3OO + CH_4 \rightleftharpoons CH_3OOH + CH_3$	4.70×10^4	2.50	21,000	($=k_4$)
24.	$CH_3OO + CH_3O \rightleftharpoons CH_3OOH + CH_2O$	3.00×10^{11}	0.0	0	[106]
25.	$CH_3OO + CH_3OH \rightleftharpoons CH_3OOH + CH_2OH$	3.98×10^{13}	0.0	19,400	($=k_{61}$)
26.	$CH_3OO + CH_2O \rightleftharpoons CH_3OOH + HCO$	4.11×10^4	2.5	10,206	($=k_{82}$)
27.	$CH_3OO + HCO \rightleftharpoons CH_3O + H + CO_2$	3.00×10^{13}	0.0	0	($=k_{90}$)
[e]28.	$CH_3OO + CH_3OO \rightleftharpoons CH_3O + CH_3O + O_2$	1.10×10^{18}	−2.40	1,800	See text, [108]
		7.00×10^{10}	0.0	800	
29.	$CH_3OO + CH_3OO \rightleftharpoons CH_3OH + CH_2O + O_2$	2.00×10^{11}	−0.55	−1,600	See text, [108]
30.	$CH_3OO + C_2H_5 \rightleftharpoons CH_3O + C_2H_5O$	5.06×10^{12}	0.0	−1,410	($=k_{22}$)
31.	$CH_3OO + C_2H_6 \rightleftharpoons CH_3OOH + C_2H_5$	1.94×10^1	3.64	17,100	[73]
[f]32.	$CH_3OOH \rightleftharpoons CH_3O + OH$	1.95×10^{35}	−6.7	47,450	[78], 1 bar
	$CH_3OOH \rightleftharpoons CH_3O + OH$	1.12×10^{28}	−4.15	46,190	10 bar
	$CH_3OOH \rightleftharpoons CH_3O + OH$	2.80×10^{26}	−3.5	46,340	50 bar
	$CH_3OOH \rightleftharpoons CH_3O + OH$	2.22×10^{17}	−0.42	44,622	k_∞
33.	$CH_3OOH + H \rightleftharpoons CH_2OOH + H_2$	5.40×10^{10}	0.0	1,860	[206], est
34.	$CH_3OOH + H \rightleftharpoons CH_3OO + H_2$	5.40×10^{10}	0.0	1,860	[206], est
35.	$CH_3OOH + H \rightleftharpoons CH_3O + H_2O$	1.20×10^{10}	0.0	1,860	[206], est

Continued

Table II Continued

	Reactions	A	β	E	Note/Ref.
36.	$CH_3OOH + O \rightleftharpoons CH_2OOH + OH$	1.61×10^{13}	0.0	4,750	[76], est
37.	$CH_3OOH + O \rightleftharpoons CH_3OO + OH$	8.65×10^{12}	0.0	4,750	[76], est
38.	$CH_3OOH + OH \rightleftharpoons CH_2OOH + H_2O$	7.23×10^{11}	0.0	−258	[76,207]
39.	$CH_3OOH + OH \rightleftharpoons CH_3OO + H_2O$	1.08×10^{12}	0.0	−437	[76,207]
40.	$CH_3OOH + HO_2 \rightleftharpoons CH_3OO + H_2O_2$	4.11×10^{4}	2.5	10,206	$(= k_{82})$
41.	$CH_2OOH \rightarrow CH_2O + OH$	2.44×10^{12}	−0.925	1,567	[208], 1 bar
	$CH_2OOH \rightarrow CH_2O + OH$	2.49×10^{13}	−0.927	1,579	10 bar
	$CH_2OOH \rightarrow CH_2O + OH$	6.95×10^{14}	−1.064	1,744	100 bar
42.	$CH_3O(+M) \rightleftharpoons CH_2O + H(+M)$	6.80×10^{13}	0.0	26,154	[118]
	Low-pressure limit:	1.87×10^{25}	−3.0	24,290	
	Troe parameters: 0.5 1000 2000 10^{30}				[g]
43.	$CH_3O + H \rightleftharpoons CH_2O + H_2$	5.31×10^{13}	0.0	745	[209]
44.	$CH_3O + H \rightleftharpoons CH_3 + OH$	4.59×10^{12}	0.0	745	[209]
45.	$CH_3O + H(+M) \rightleftharpoons CH_3OH(+M^h)$	2.43×10^{12}	0.515	50	[136]
	Low-pressure limit:	4.66×10^{41}	−7.44	14,080	
	Troe parameters: 0.7 100 9×10^5 10^5				
46.	$CH_3O + O \rightleftharpoons CH_2O + OH$	3.76×10^{12}	0.0	0	[76,210]
47.	$CH_3O + OH \rightleftharpoons CH_2O + H_2O$	1.80×10^{13}	0.0	0	[106]
48.	$CH_3O + HO_2 \rightleftharpoons CH_2O + H_2O_2$	3.00×10^{11}	0.0	0	[106]
49.	$CH_3O + O_2 \rightleftharpoons CH_2O + HO_2$	2.17×10^{10}	0.0	1,750	[211]
50.	$CH_3O + CO \rightleftharpoons CH_3 + CO_2$	9.54×10^{25}	−4.93	9,080	[212]
51.	$CH_3O + CH_4 \rightleftharpoons CH_3OH + CH_3$	1.32×10^{14}	0.0	15,070	[119]
52.	$CH_3O + CH_3 \rightleftharpoons CH_2O + CH_4$	2.40×10^{13}	0.0	0	[106]
53.	$CH_3O + CH_2O \rightleftharpoons CH_3OH + HCO$	1.02×10^{11}	0.0	2,980	[106]
54.	$CH_3O + CH_3O \rightleftharpoons CH_3OH + CH_2O$	6.03×10^{13}	0.0	0	[106]
55.	$CH_3OH + H \rightleftharpoons CH_2OH + H_2$	2.92×10^{9}	1.24	4,490	[62,76]
56.	$CH_3OH + H \rightleftharpoons CH_3O + H_2$	5.15×10^{8}	1.24	4,490	[62,76]
57.	$CH_3OH + O \rightleftharpoons CH_2OH + OH$	2.10×10^{13}	0.0	5,305	[62,76]
58.	$CH_3OH + O \rightleftharpoons CH_3O + OH$	3.70×10^{12}	0.0	5,305	[62,76]
59.	$CH_3OH + OH \rightleftharpoons CH_2OH + H_2O$	1.50×10^{8}	1.4434	113	[62]
60.	$CH_3OH + OH \rightleftharpoons CH_3O + H_2O$	2.70×10^{7}	1.4434	113	[62]
61.	$CH_3OH + HO_2 \rightleftharpoons CH_2OH + H_2O_2$	2.00×10^{13}	0.0	15,000	[62]
62.	$CH_3OH + O_2 \rightleftharpoons CH_2OH + HO_2$	6.10×10^{13}	0.0	46,600	[62]
63.	$CH_2OH(+M) \rightleftharpoons CH_2O + H(+M^i)$	2.80×10^{14}	−0.73	32,820	[213]
	Low-pressure limit:	6.01×10^{33}	−5.39	36,200	
	Troe parameters: 0.96 67.6 1855 7543				
64.	$CH_2OH + H(+M) \rightleftharpoons CH_3OH(+M)$	4.34×10^{15}	−0.79	0	$(=k_8)$
	Low-pressure limit:	3.84×10^{37}	−6.21	1,333	
	Troe parameters: 0.25 210 1434 10^{30}				
65.	$CH_2OH + H \rightleftharpoons CH_2O + H_2$	1.40×10^{13}	0.0	0	[62]
66.	$CH_2OH + H \rightleftharpoons CH_3 + OH$	6.00×10^{12}	0.0	0	[62]
67.	$CH_2OH + O \rightleftharpoons CH_2O + OH$	6.56×10^{13}	0.0	−693	[214]
68.	$CH_2OH + OH \rightleftharpoons CH_2O + H_2O$	2.40×10^{13}	0.0	0	[215]
69.	$CH_2OH + HO_2 \rightleftharpoons CH_2O + H_2O_2$	1.20×10^{13}	0.0	0	[215]
[f]70.	$CH_2OH + O_2 \rightleftharpoons CH_2O + HO_2$	7.23×10^{13}	0.0	3,736	[76]
		2.89×10^{16}	−1.5	0	
71.	$CH_2OH + CH_4 \rightleftharpoons CH_3OH + CH_3$	2.16×10^{1}	3.1	16,227	[215]
72.	$CH_2OH + HCO \rightleftharpoons CH_3OH + CO$	1.00×10^{13}	0.0	0	[62]
73.	$CH_2OH + HCO \rightleftharpoons CH_2O + CH_2O$	1.50×10^{13}	0.0	0	[216]
74.	$CH_2OH + CH_2O \rightleftharpoons CH_3OH + HCO$	5.48×10^{3}	2.81	5,862	[215]
75.	$CH_2OH + CH_2OH \rightleftharpoons CH_3OH + CH_2O$	4.82×10^{12}	0.0	0	[215]
76.	$CH_2OH + CH_3O \rightleftharpoons CH_3OH + CH_2O$	2.41×10^{12}	0.0	0	[215]

Continued

Table II Continued

	Reactions	A	β	E	Note/Ref.
77.	$CH_2O(+M) \rightleftharpoons HCO + H(+M)$	8.00×10^{15}	0.0	87,730	[217]
	Low-pressure limit:	3.73×10^{15}	0.0	73,480	
78.	$CH_2O(+M) \rightleftharpoons CO + H_2(+M)$	3.70×10^{13}	0.0	71,970	[217]
	Low-pressure limit:	5.66×10^{15}	0.0	65,850	
79.	$CH_2O + H \rightleftharpoons HCO + H_2$	4.10×10^{8}	1.47	2,444	[76]
80.	$CH_2O + O \rightleftharpoons HCO + OH$	4.16×10^{11}	0.57	2,760	[76]
81.	$CH_2O + OH \rightleftharpoons HCO + H_2O$	7.82×10^{7}	1.63	−1,055	[122]
82.	$CH_2O + HO_2 \rightleftharpoons HCO + H_2O_2$	4.11×10^{4}	2.5	10,206	[121]
83.	$CH_2O + O_2 \rightleftharpoons HCO + HO_2$	2.44×10^{5}	2.5	36,460	[76]
84.	$CH_2O + CH_3 \rightleftharpoons HCO + CH_4$	3.19×10^{1}	3.36	4,310	[76]
85.	$HCO \rightleftharpoons H + CO$	$P[\text{bar}]^{0.865} \times 9.83 \times 10^{11}$	−0.865	16,755	[125]
86.	$HCO + H \rightleftharpoons CO + H_2$	1.10×10^{14}	0.0	0	[218]
87.	$HCO + O \rightleftharpoons CO + OH$	3.00×10^{13}	0.0	0	[76]
88.	$HCO + O \rightleftharpoons CO_2 + H$	3.00×10^{13}	0.0	0	[76]
89.	$HCO + OH \rightleftharpoons CO + H_2O$	1.08×10^{14}	0.0	0	[76]
90.	$HCO + HO_2 \rightleftharpoons CO_2 + OH + H$	3.00×10^{13}	0.0	0	[106]
91.	$HCO + O_2 \rightleftharpoons CO + HO_2$	2.71×10^{10}	0.68	−469	[76]
92.	$HCO + CH_3 \rightleftharpoons CO + CH_4$	2.80×10^{13}	0.0	0	[219]
93.	$HCO + HCO \rightleftharpoons CO + CH_2O$	2.70×10^{13}	0.0	0	[218]

Parameters for use in the modified Arrhenius expression $k = AT^{\beta} \exp(-E/[RT])$.
Units are mol, cm, s, cal.
[a] Enhanced third-body efficiencies: $CH_4 = 1.9$, $C_2H_6 = 4.8$.
[b] Fitted to $F_{\text{cent},8} = -0.756 \exp\left(\frac{-70.7}{T}\right) + \exp\left(\frac{-T}{5646}\right)$ [101] in [76].
[c] Expressed as the sum of the rate constants at a given pressure.
[d] Fitted to original expression from [81].
[e] Expressed as the sum of the rate constants.
[f] Arrhenius parameters fitted to discrete data points from [78].
[g] Fitted to $F_{\text{cent,R42}} = 0.97 - \frac{T}{1950}$ [118].
[h] Enhanced third-body efficiencies: $Ar = 0.7$, $H_2 = 2$, $H_2O = 6$, $CH_4 = 3$, $CO = 1.5$, $CO_2 = 2$, $C_2H_6 = 3$.
[i] Enhanced third-body efficiencies: $H_2 = 2$, $H_2O = 5$, $CO = 2$, $CO_2 = 3$.

dependence of the high-pressure limit. Shock tube experiments [90–92], supported by theoretical studies [93,94], indicate a slightly negative temperature dependence, whereas other data [95–97], including the preferred expression from Baulch et al. [76], advocate a temperature independent high-pressure limit.

The reaction between CH_3 and O-atoms forms mainly CH_2O+H (R6), with a minor yield of H_2+CO+H (R7) [98,99]. We rely on the overall rate constant from Baulch et al. [76] together with the latest measurement of the branching ratio [100]. The reaction of CH_3 with OH proceeds through an excited CH_3OH^* adduct that may be collisionally stabilized to CH_3OH (R8), or decompose to a number of products, e.g. $^1CH_2$+H_2O, $^3CH_2$+H_2O, CH_2O+H_2, HCOH+H_2, and CH_2OH+H [101,102]. The overall rate constant is fairly well established, but in the low-pressure and falloff region, branching ratios are uncertain and reported values deviate significantly [101, 103–105]. The preferred rate constant for the stabilization channel k_8 is taken from the study by De Avillez Pereira et al. [101] with He as bath gas. Their analysis indicated that the bimolecular channels to $^1CH_2 + H_2O$ and $HCOH + H_2$ both exhibit a strong negative dependence of pressure, which makes them unlikely to gain importance at the conditions relevant to the present study.

Alkyl peroxide species are characteristic intermediates in the hydrocarbon oxidation chain at high pressure and/or low to intermediate temperatures due to the importance of the addition/stabilization reactions between alkyl radicals (CH_3, C_2H_5, etc.) and molecular oxygen. However, only a few of these reactions have been characterized experimentally above room temperature. As a consequence, available recommendations are often based either on extrapolations from atmospheric chemistry research, where peroxide species also play important roles, or from simple analogies with, e.g. hydroperoxide chemistry [76,106]. The bond strengths of HOO—H ($D_{298} = 87.5$ kcal/mol [65]) and CH_3OO—H (87.8 kcal/mol [67]) are very similar. This indicates that analogue H-abstraction reactions from the peroxy-group of H_2O_2 and CH_3OOH exhibit comparable rates. However, the O—O bond in HO—OH

(D_{298} = 51.3 kcal/mol [107]) is stronger than that of CH_3O—OH (~42.6 kcal/mol [66]), indicating that reactions of alkylperoxide involving O—O bond cleavage could be somewhat faster than the analogue reactions with hydroperoxides. In the present study, rate constants for alkyl peroxide reactions are occasionally estimated from analogy with hydroperoxide reactions without any corrections to compensate for the difference in O—O bond strength.

Methylperoxyl radicals (CH_3OO) are typically converted through an addition/elimination mechanism involving cleavage of the weak O—O bond. This mechanism can be a fast radical–radical exchange, to form CH_3O and another oxygenated radical, or radical termination yielding two or more stable products via H atom shift within the peroxide adduct before O—O bond cleavage. The most important reactions of CH_3OO under the present conditions are those with HO_2 and CH_3. For CH_3OO+HO_2 we adopt the overall rate constant of Tyndall et al. [108], assuming $CH_3OOH + O_2$ (R20) to be the dominating product channel [109–111]. For the reaction with CH_3 to form $CH_3O + CH_3O$ (R22), we rely on the results of Keiffer et al. [112,113], in good agreement with room temperature data [114,115].

Methylperoxyl radicals (CH_3OO) may also be consumed through H-abstraction from a stable molecule, e.g. CH_4 (R23) or CH_2O (R26), to form CH_3OOH and a new radical. Since CH_3OOH is typically consumed through unimolecular decomposition at the O—O bond to CH_3O and OH radicals, this sequence results in a net gain of reactive compounds and overall reactivity of the chemical system at hand. In the absence of measurements for these steps, rate constants were estimated by analogy with HO_2 reactions. The self-reaction of CH_3OO may involve radical termination, $CH_3OH + CH_2O + O_2$ (R29), or propagation, $CH_3O + CH_3O + O_2$ (R28). The reaction has been extensively studied; the values of k_{28} and k_{29} in Table II are fitted expressions based on the results of Tyndall et al. [108], who reinterpreted much of the earlier work.

A number of potential CH_3OOH conversion channels are included in the mechanism, but at the temperature and pressure ranges of interest, the most important path is the thermal decomposition (R32). The pressure-dependent rate constants provided in Table II are fitted expressions to discrete values of $k_{CH_3OOH\rightarrow prod}$ given by Zhu and Lin [78]. Their values of k_{32}, derived from variational RRKM theory, are in good agreement with reported measurements [116,117]. It is expected that the reaction is close to the high-pressure limit at 100 bar.

Most reactions of CH_3O and CH_2OH are treated in detail elsewhere [62], and only a few reactions are discussed here. Thermal dissociation of CH_3O (R42) is now well characterized over a wide range of temperature and pressure [118]. The H-abstraction reaction from CH_4 by CH_3O (R51) is the most important source of CH_3OH in fuel-rich oxidation of natural gas. If the predominant collision partner is CH_4, formation of CH_3OH via (R51) may compete with the decomposition of CH_3O via (R42) at medium temperatures. Despite the importance under reducing conditions, only few experimental studies of (R51) are available. The preferred rate constant is the determination by Wantuck et al. [119], who measured the overall removal rate of CH_3O at 673–973 K in atmospheres containing either CH_4 or an inert gas. Their results are in reasonable agreement with the early data of Shaw and Thynne [120] obtained at 403–523 K. Rate expressions for reactions of CH_3O with CH_3 (R52) and CH_2O (R53), as well as the self-reaction with CH_3O to $CH_3OH + CH_2O$ (R54), all follow the recommendations by Tsang and Hampson [106]. The addition/stabilization channels to dimethylether (CH_3OCH_3) and dimethylperoxide (CH_3OOCH_3) are neglected in the present work.

The rate constants for most reactions in the CH_2O subset are known with considerable accuracy. These include reaction of CH_2O with H (R79), O (R80), HO_2 (R82), and CH_3 (R84) [76,121]. The data for $CH_2O + OH$ (R81) show some scatter, especially at higher temperatures [76]. We have adopted the rate constant from Vasudevan et al. [122], based on their shock tube measurements and low-temperature measurements from Sivakumaran et al. [123]. For $CH_2O + O_2$ (R83), we follow the recommendation of Baulch et al. [76], which is in excellent agreement with the most recent high-temperature expression of Vasudevan et al. [124].

The reactions of HCO are discussed in detail elsewhere [62]. The most important steps are the thermal dissociation (R85) and the reaction with O_2 (R91). Despite several recent studies of these reactions, both rate constants are still in controversy. For HCO(+M), we adopt the rate coefficients of Hippler et al. [125,126], with an estimated accuracy of ±30% at 500–1000 K and 0.01–100 bar of N_2. For the reaction between HCO and O_2 (R91), the most reliable rate constants are those advocated by Baulch et al. [76] and DeSain et al. [127], but recent shock tube results by Colberg and Friedrichs [128] indicate that more work is desirable on the rate constant at intermediate to high temperatures.

C_2 Hydrocarbon Subset

Table III shows the proposed C_2 hydrocarbon subset. For reactions of C_2H_6, we rely mostly on the recommendations of Baulch et al. [76]. The reactions with H (R94), OH (R96), and CH_3 (R99) are well

Table III Reactions from the C_2 Hydrocarbon Reaction Mechanism

	Reactions	A	β	E	Note/Ref.
94.	$C_2H_6 + H \rightleftharpoons C_2H_5 + H_2$	9.82×10^{13}	0.0	9,220	[76]
95.	$C_2H_6 + O \rightleftharpoons C_2H_5 + OH$	1.14×10^{-7}	6.5	274	[129]
96.	$C_2H_6 + OH \rightleftharpoons C_2H_5 + H_2O$	9.15×10^{6}	2.0	990	[168]
97.	$C_2H_6 + HO_2 \rightleftharpoons C_2H_5 + H_2O_2$	1.10×10^{5}	2.5	16,850	[76]
98.	$C_2H_6 + O_2 \rightleftharpoons C_2H_5 + HO_2$	7.29×10^{5}	2.5	49,160	[76]
[a]99.	$C_2H_6 + CH_3 \rightleftharpoons C_2H_5 + CH_4$	5.60×10^{10}	0.0	9,418	[76]
		8.43×10^{14}	0.0	22,250	
100.	$C_2H_5 + H(+M) \rightleftharpoons C_2H_6(+M^b)$	5.21×10^{17}	−0.99	1,580	[136,220]
	Low-pressure limit:	1.99×10^{41}	−7.08	6,685	
	Troe parameters: 0.8422 125 2219 6882				
101.	$C_2H_5 + O \rightleftharpoons CH_3 + CH_2O$	4.24×10^{13}	0.0	0	[138]
102.	$C_2H_5 + O \rightleftharpoons CH_3CHO + H$	5.32×10^{13}	0.0	0	[138]
103.	$C_2H_5 + O \rightleftharpoons C_2H_4 + OH$	3.06×10^{13}	0.0	0	[138]
104.	$C_2H_5 + OH \rightleftharpoons C_2H_4 + H_2O$	2.40×10^{13}	0.0	0	[106]
105.	$C_2H_5 + HO_2 \rightleftharpoons C_2H_5O + OH$	3.10×10^{13}	0.0	0	[134]
106.	$C_2H_5 + O_2(+M) \rightleftharpoons C_2H_5OO(+M)$	2.02×10^{10}	0.98	−64	[133]
	Low-pressure limit:	8.49×10^{29}	−4.29	220	
	Troe parameters: 0.897 10^{-30} 601 10^{30}				
107.	$C_2H_5 + O_2 \rightleftharpoons C_2H_4 + HO_2$	1.41×10^{7}	1.09	−1,975	(=k_0 [133])
108.	$C_2H_5 + CH_3 \rightleftharpoons C_2H_4 + CH_4$	9.03×10^{11}	0.0	0	[76]
109.	$C_2H_5 + HCO \rightleftharpoons C_2H_6 + CO$	4.34×10^{13}	0.0	0	[221]
110.	$C_2H_4(+M) \rightleftharpoons C_2H_2 + H_2(+M^b)$	8.00×10^{12}	0.44	88,770	[136]
	Low-pressure limit:	1.58×10^{51}	−9.3	97,800	
	Troe parameters: 0.735 180 1035 5417				
111.	$C_2H_4 + H \rightleftharpoons C_2H_3 + H_2$	2.35×10^{2}	3.62	11,266	[76]
112.	$C_2H_4 + H(+M) \rightleftharpoons C_2H_5(+M)$	3.97×10^{9}	1.28	1,292	[76]
	Low-pressure limit:	4.71×10^{18}	0.0	755	
	Troe parameters: 0.76 40 1025 10^{30}				
[a]113.	$C_2H_4 + O \rightleftharpoons CH_3 + HCO$	3.86×10^{12}	0.0	1,494	[181]
		6.23×10^{13}	0.0	6,855	
[a]114.	$C_2H_4 + O \rightleftharpoons CH_2CHO + H$	1.74×10^{12}	0.0	1,494	[181]
		2.80×10^{13}	0.0	6,855	
115.	$C_2H_4 + OH(+M) \rightleftharpoons 2\text{-}C_2H_4OH(+M)$	2.26×10^{5}	2.28	−2,466	[177]
	Low-pressure limit:	5.02×10^{19}	−8.87	2,470	[c]
116.	$C_2H_4 + OH \rightleftharpoons H_2CCHOH + H$	6.08×10^{7}	1.38	1,615	[177]
117.	$C_2H_4 + OH \rightleftharpoons C_2H_3 + H_2O$	7.17×10^{0}	3.71	435	[177]
118.	$C_2H_4 + O_2 \rightleftharpoons CH_2CHO + OH$	3.50×10^{7}	1.8	39,000	See text, [193]
119.	$C_2H_4 + O_2 \rightleftharpoons CH_2O + CH_2O$	3.50×10^{7}	1.8	39,000	See text, [193]
120.	$C_2H_4 + CH_3 \rightleftharpoons C_2H_3 + CH_4$	6.00×10^{7}	1.56	16,630	[76]
121.	$C_2H_3 + H(+M) \rightleftharpoons C_2H_4(+M)$	3.88×10^{13}	0.20	0	[222]
	Low-pressure limit:	2.10×10^{24}	−1.3	0	[223]
	Troe parameters: 0.5 10^{-30} 10^{30} 10^{30}				
122.	$C_2H_3 + H \rightleftharpoons C_2H_2 + H_2$	4.50×10^{13}	0.0	0	[223]
123.	$C_2H_3 + O \rightleftharpoons CH_2CO + H$	3.00×10^{13}	0.0	0	[76]
124.	$C_2H_3 + OH \rightleftharpoons C_2H_2 + H_2O$	2.00×10^{13}	0.0	0	[224]
125.	$C_2H_3 + HO_2 \rightleftharpoons CH_2CHO + OH$	3.00×10^{13}	0.0	0	[106]
126.	$C_2H_3 + O_2 \rightleftharpoons CH_2O + HCO$	3.85×10^{12}	0.0	−238	[76]
127.	$C_2H_3 + CH_3 \rightleftharpoons C_2H_2 + CH_4$	2.10×10^{13}	0.0	0	[225]
128.	$C_2H_3 + HCO \rightleftharpoons C_2H_4 + CO$	9.00×10^{13}	0.0	0	[106]
129.	$C_2H_5OO(+M) \rightleftharpoons C_2H_4 + HO_2(+M)$	7.14×10^{4}	2.32	27,955	[133]

Continued

Table III Continued

	Reactions	A	β	E	Note/Ref.
	Low-pressure limit:	8.31×10^{21}	−0.651	22,890	
	Troe parameters: 1.0 10^{-30} 106 10^{30}				
130.	$C_2H_5OO + H \rightleftharpoons C_2H_5O + OH$	9.64×10^{13}	0.0	0	($=k_{16}$)
131.	$C_2H_5OO + O \rightleftharpoons C_2H_5O + O_2$	1.63×10^{13}	0.0	−445	($=k_{17}$)
132.	$C_2H_5OO + OH \rightleftharpoons C_2H_5OH + O_2$	2.00×10^{15}	−0.6	0	($=k_{18}$)
133.	$C_2H_5OO + OH \rightleftharpoons C_2H_5O + HO_2$	4.00×10^{11}	0.6	0	($=k_{19}$)
134.	$C_2H_5OO + HO_2 \rightleftharpoons C_2H_5OOH + O_2$	4.50×10^{11}	0.0	−1,391	[108]
135.	$C_2H_5OO + CO \rightleftharpoons C_2H_5O + CO_2$	6.92×10^{6}	1.61	17,500	($=k_{135}$)
136.	$C_2H_5OO + CH_3 \rightleftharpoons C_2H_5O + CH_3O$	5.06×10^{12}	0.0	−1,411	($=k_{22}$)
137.	$C_2H_5OO + CH_4 \rightleftharpoons C_2H_5OOH + CH_3$	4.70×10^{4}	2.5	21,000	($=k_4$)
138.	$C_2H_5OO + CH_3OH \rightleftharpoons C_2H_5OOH + CH_2OH$	3.98×10^{13}	0.0	19,400	($=k_{25}$)
139.	$C_2H_5OO + CH_2O \rightleftharpoons C_2H_5OOH + HCO$	4.11×10^{4}	2.5	10,206	($=k_{26}$)
140.	$C_2H_5OO + C_2H_5 \rightleftharpoons C_2H_5O + C_2H_5O$	5.06×10^{12}	0.0	−1,411	($=k_{22}$)
141.	$C_2H_5OO + C_2H_6 \rightleftharpoons C_2H_5OOH + C_2H_5$	8.60×10^{0}	3.76	17,200	[73]
142.	$C_2H_5OO + CH_3CHO \rightleftharpoons C_2H_5OOH + CH_3CO$	2.40×10^{19}	−2.2	14,030	($=k_{198}$)
143.	$C_2H_5OO + CH_3CHO \rightleftharpoons C_2H_5OOH + CH_2CHO$	2.32×10^{11}	0.4	14,864	($=k_{199}$)
144.	$C_2H_5OO + C_2H_5OO \rightleftharpoons C_2H_5O + C_2H_5O + O_2$	2.85×10^{11}	−0.27	408	See text, [147]
145.	$C_2H_5OO + C_2H_5OO \rightleftharpoons CH_3CHO + C_2H_5OH + O_2$	4.27×10^{9}	0.0	−850	See text, [147]
146.	$C_2H_5OOH \rightleftharpoons C_2H_5O + OH$	1.95×10^{35}	−6.7	47,450	($=k_{32}$), 1 bar
	$C_2H_5OOH \rightleftharpoons C_2H_5O + OH$	1.12×10^{28}	−4.15	46,190	10 bar
	$C_2H_5OOH \rightleftharpoons C_2H_5O + OH$	2.80×10^{26}	−3.5	46,340	50 bar
	$C_2H_5OOH \rightleftharpoons C_2H_5O + OH$	2.22×10^{17}	−0.42	44,622	k_∞
147.	$C_2H_5OOH + H \rightleftharpoons CH_3CHOOH + H_2$	6.48×10^{10}	0.0	1,860	($=k_{33}$)
148.	$C_2H_5OOH + H \rightleftharpoons C_2H_5OO + H_2$	4.32×10^{10}	0.0	1,860	($=k_{34}$)
149.	$C_2H_5OOH + H \rightleftharpoons C_2H_5O + H_2O$	1.20×10^{10}	0.0	1,860	($=k_{35}$)
150.	$C_2H_5OOH + O \rightleftharpoons CH_3CHOOH + OH$	1.61×10^{13}	0.0	4,750	($=k_{36}$)
151.	$C_2H_5OOH + O \rightleftharpoons C_2H_5OO + OH$	8.65×10^{12}	0.0	4,750	($=k_{37}$)
152.	$C_2H_5OOH + OH \rightleftharpoons CH_3CHOOH + H_2O$	7.23×10^{11}	0.0	−258	($=k_{38}$)
153.	$C_2H_5OOH + OH \rightleftharpoons C_2H_5OO + H_2O$	1.08×10^{12}	0.0	−437	($=k_{39}$)
154.	$C_2H_5OOH + HO_2 \rightleftharpoons C_2H_5OO + H_2O_2$	4.11×10^{4}	2.5	10,206	($= k_{82}$)
155.	$CH_3CHOOH \rightarrow CH_3CHO + OH$	3.50×10^{12}	−0.947	979	[208], 1 bar
	$CH_3CHOOH \rightarrow CH_3CHO + OH$	3.50×10^{13}	−0.947	980	10 bar
	$CH_3CHOOH \rightarrow CH_3CHO + OH$	5.75×10^{14}	−1.012	1,068	100 bar
156.	$C_2H_5O(+M) \rightleftharpoons CH_3 + CH_2O(+M)$	1.10×10^{13}	0.0	16,790	[165]
	Low-pressure limit:	2.00×10^{16}	0.0	13,970	
	Troe parameters: 0.78 10^{-30} 1235 10^{30}				
157.	$C_2H_5O \rightleftharpoons CH_3CHO + H$	1.30×10^{13}	0.0	20,060	($=k_\infty$ [165])
158.	$C_2H_5O + H \rightleftharpoons CH_3CHO + H_2$	3.00×10^{13}	0.0	0	est
159.	$C_2H_5O + OH \rightleftharpoons CH_3CHO + H_2O$	3.00×10^{13}	0.0	0	est
160.	$C_2H_5O + O_2 \rightleftharpoons CH_3CHO + HO_2$	1.45×10^{10}	0.0	645	[174]
161.	$C_2H_5O + CO \rightleftharpoons C_2H_5 + CO_2$	9.54×10^{25}	−4.93	9,080	($=k_{50}$)
162.	$C_2H_5OH(+M) \rightleftharpoons CH_2OH + CH_3(+M^d)$	5.94×10^{23}	−1.68	91,163	[143]
	Low-pressure limit:	2.88×10^{85}	−18.9	109,914	
	Troe parameters: 0.5 200 890 4600				
163.	$C_2H_5OH(+M) \rightleftharpoons C_2H_5 + OH(+M^d)$	1.25×10^{23}	−1.54	96,005	[143]
	Low-pressure limit:	3.25×10^{85}	−18.81	114,930	
	Troe parameters: 0.5 300 900 5000				
164.	$C_2H_5OH(+M) \rightleftharpoons C_2H_4 + H_2O(+M^e)$	2.79×10^{13}	0.090	66,136	[143]
	Low-pressure limit:	2.57×10^{83}	−18.85	86,452	
	Troe parameters: 0.7 350 800 3800				
165.	$C_2H_5OH(+M) \rightleftharpoons CH_3CHO + H_2(+M^e)$	7.24×10^{11}	0.095	91,007	[143]
	Low-pressure limit:	4.46×10^{87}	−19.42	115,586	
	Troe parameters: 0.9 900 1100 3500				

Continued

Table III Continued

	Reactions	A	β	E	Note/Ref.
166.	$C_2H_5OH + H \rightleftharpoons 1\text{-}C_2H_4OH + H_2$	2.58×10^7	1.65	2,827	[143]
167.	$C_2H_5OH + H \rightleftharpoons 2\text{-}C_2H_4OH + H_2$	1.23×10^7	1.8	5,098	[143]
168.	$C_2H_5OH + H \rightleftharpoons C_2H_5O + H_2$	1.50×10^7	1.65	3,038	[143]
169.	$C_2H_5OH + O \rightleftharpoons 1\text{-}C_2H_4OH + OH$	1.88×10^7	1.85	1,824	[143]
170.	$C_2H_5OH + O \rightleftharpoons 2\text{-}C_2H_4OH + OH$	9.41×10^7	1.7	5,459	[143]
171.	$C_2H_5OH + O \rightleftharpoons C_2H_5O + OH$	1.58×10^7	2.0	4,448	[143]
172.	$C_2H_5OH + OH \rightleftharpoons 1\text{-}C_2H_4OH + H_2O$	4.64×10^{11}	0.15	0	[143]
173.	$C_2H_5OH + OH \rightleftharpoons 2\text{-}C_2H_4OH + H_2O$	1.74×10^{11}	0.27	600	[143]
174.	$C_2H_5OH + OH \rightleftharpoons C_2H_5O + H_2O$	7.46×10^{11}	0.3	1,634	[143]
175.	$C_2H_5OH + HO_2 \rightleftharpoons 1\text{-}C_2H_4OH + H_2O_2$	8.20×10^3	2.55	10,750	[143]
176.	$C_2H_5OH + HO_2 \rightleftharpoons 2\text{-}C_2H_4OH + H_2O_2$	1.23×10^4	2.55	15,750	[143]
177.	$C_2H_5OH + HO_2 \rightleftharpoons C_2H_5O + H_2O_2$	2.50×10^{12}	0.0	24,000	[143]
178.	$C_2H_5OH + CH_3 \rightleftharpoons 1\text{-}C_2H_4OH + CH_4$	7.28×10^2	2.99	7,948	[143]
179.	$C_2H_5OH + CH_3 \rightleftharpoons 2\text{-}C_2H_4OH + CH_4$	2.19×10^2	3.18	9,622	[143]
180.	$C_2H_5OH + CH_3 \rightleftharpoons C_2H_5O + CH_4$	1.45×10^2	2.99	7,649	[143]
181.	$1\text{-}C_2H_4OH + M \rightleftharpoons CH_3CHO + H + M$	1.00×10^{14}	0.0	25,000	[143]
182.	$1\text{-}C_2H_4OH + O \rightleftharpoons CH_3CHO + OH$	1.00×10^{14}	0.0	0	[143]
183.	$1\text{-}C_2H_4OH + H \rightleftharpoons CH_2OH + CH_3$	3.00×10^{13}	0.0	0	[143]
184.	$1\text{-}C_2H_4OH + H \rightleftharpoons C_2H_4 + H_2O$	3.00×10^{13}	0.0	0	[143]
185.	$1\text{-}C_2H_4OH + OH \rightleftharpoons CH_3CHO + H_2O$	5.00×10^{12}	0.0	0	[143]
186.	$1\text{-}C_2H_4OH + HO_2 \rightleftharpoons CH_3CHO + OH + OH$	4.00×10^{13}	0.0	0	[143]
[a]187.	$1\text{-}C_2H_4OH + O_2 \rightleftharpoons CH_3CHO + HO_2$	8.43×10^{15}	−1.2	0	[143]
		4.82×10^{14}	0.0	5,017	
188.	$2\text{-}C_2H_4OH + O_2 \rightleftharpoons HOC_2H_4O_2$	1.00×10^{12}	0.0	−1,100	[143]
189.	$HOC_2H_4O_2 \rightleftharpoons CH_2O + CH_2O + OH$	6.00×10^{10}	0.0	24,500	[143]
190.	$CH_3CHO(+M) \rightleftharpoons CH_3 + HCO(+M)$	4.29×10^{22}	−1.88	85,480	[226]
	Low-pressure limit:	2.22×10^{76}	−11.81	95,040	
	Troe parameters: 0.23 80 7000 10^{30}				[f]
191.	$CH_3CHO + H \rightleftharpoons CH_3CO + H_2$	4.66×10^{13}	−0.35	3,000	[143,227]
192.	$CH_3CHO + H \rightleftharpoons CH_2CHO + H_2$	1.85×10^{12}	0.4	5,359	[143,227]
193.	$CH_3CHO + O \rightleftharpoons CH_3CO + OH$	1.77×10^{18}	−1.9	2,975	[143,227]
194.	$CH_3CHO + O \rightleftharpoons CH_2CHO + OH$	3.72×10^{13}	−0.2	3,556	[143,227]
195.	$CH_3CHO + OH \rightleftharpoons CH_3CO + H_2O$	2.35×10^{11}	0.3	−1,000	[228,229][g]
196.	$CH_3CHO + OH \rightleftharpoons CH_2CHO + H_2O$	3.00×10^{13}	−0.6	800	[228,229][g]
197.	$CH_3CHO + O_2 \rightleftharpoons CH_3CO + HO_2$	1.20×10^5	2.5	37,550	[76]
198.	$CH_3CHO + HO_2 \rightleftharpoons CH_3CO + H_2O_2$	2.40×10^{19}	−2.2	14,030	[143,227]
199.	$CH_3CHO + HO_2 \rightleftharpoons CH_2CHO + H_2O_2$	2.32×10^{11}	0.4	14,864	[143,227]
200.	$CH_3CHO + CH_3 \rightleftharpoons CH_3CO + CH_4$	3.90×10^{-7}	5.8	2,200	[143,227]
201.	$CH_3CHO + CH_3 \rightleftharpoons CH_2CHO + CH_4$	2.45×10^1	3.15	5,727	[143,227]
202.	$CH_3CO \rightleftharpoons CH_3 + CO$	6.45×10^{18}	−2.52	16,436	[230], 1 bar
	$CH_3CO \rightleftharpoons CH_3 + CO$	8.18×10^{19}	−2.55	17,263	10 bar
	$CH_3CO \rightleftharpoons CH_3 + CO$	1.26×10^{20}	−2.32	18,012	100 bar
	$CH_3CO \rightleftharpoons CH_3 + CO$	1.07×10^{12}	0.63	16,895	k_∞
203.	$CH_3CO + H \rightleftharpoons CH_3 + HCO$	2.10×10^{13}	0.0	0	[231,232]
204.	$CH_3CO + H \rightleftharpoons CH_2CO + H_2$	1.20×10^{13}	0.0	0	[231,232]
205.	$CH_3CO + O \rightleftharpoons CH_3 + CO_2$	1.60×10^{14}	0.0	0	[76]
206.	$CH_3CO + O \rightleftharpoons CH_2CO + OH$	5.30×10^{13}	0.0	0	[76]
207.	$CH_3CO + OH \rightleftharpoons CH_2CO + H_2O$	1.20×10^{13}	0.0	0	[106]
208.	$CH_3CO + CH_3OO \rightleftharpoons CH_3 + CO_2 + CH_3O$	2.40×10^{13}	0.0	0	[106]
209.	$CH_3CO + CH_3 \rightleftharpoons C_2H_6 + CO$	3.26×10^{13}	0.0	0	[233]
210.	$CH_3CO + CH_3 \rightleftharpoons CH_2CO + CH_4$	5.33×10^{13}	0.0	0	[233]
211.	$CH_3CO + O_2 \rightleftharpoons CH_2O + CO + OH$	1.93×10^{12}	0.0	0	[234]
212.	$CH_2CHO \rightleftharpoons CH_3 + CO$	1.17×10^{43}	−9.83	43,756	[143], 1 bar

Continued

Table III Continued

	Reactions	A	β	E	Note/Ref.
213.	$CH_2CHO \rightleftharpoons CH_2CO + H$	1.81×10^{43}	−9.61	45,868	[143], 1 bar
214.	$CH_2CHO \rightleftharpoons CH_3CO$	2.80×10^{37}	−7.393	57,015	[208], 1 bar
	$CH_2CHO \rightleftharpoons CH_3CO$	6.40×10^{32}	−5.877	55,941	10 bar
	$CH_2CHO \rightleftharpoons CH_3CO$	1.02×10^{16}	−0.654	50,433	100 bar
215.	$CH_2CHO + H \rightleftharpoons CH_3 + HCO$	5.00×10^{13}	0.0	0	[143]
216.	$CH_2CHO + H \rightleftharpoons CH_2CO + H_2$	2.00×10^{13}	0.0	0	[143]
217.	$CH_2CHO + O \rightleftharpoons CH_2O + HCO$	1.00×10^{14}	0.0	0	[235]
218.	$CH_2CHO + OH \rightleftharpoons CH_2CO + H_2O$	3.00×10^{13}	0.0	0	[235]
219.	$CH_2CHO + O_2 \rightleftharpoons CH_2O + CO + OH$	5.66×10^{17}	−1.757	11,067	[208], 1 bar
	$CH_2CHO + O_2 \rightleftharpoons CH_2O + CO + OH$	1.05×10^{14}	−0.610	11,422	10 bar
	$CH_2CHO + O_2 \rightleftharpoons CH_2O + CO + OH$	1.50×10^{-10}	6.690	4,868	100 bar
220.	$CH_2CHO + CH_3 \rightleftharpoons C_2H_5 + CO + H$	4.90×10^{14}	−0.50	0	[235]
221.	$CH_2CHO + HO_2 \rightleftharpoons CH_2O + HCO + OH$	7.00×10^{12}	−0.50	0	[143]
222.	$CH_2CHO + HO_2 \rightleftharpoons CH_3CHO + O_2$	3.00×10^{12}	−0.50	0	[143]
223.	$CH_2CO + H \rightleftharpoons CH_2CHO$	1.99×10^{9}	1.43	6,050	[230], k_∞
224.	$CH_2CO + H \rightleftharpoons CH_3CO$	2.30×10^{8}	1.61	2,627	[230], k_∞
225.	$CH_2CO + H \rightleftharpoons CH_3 + CO$	3.30×10^{10}	0.851	2,840	[236]
226.	$CH_2CO + H \rightleftharpoons HCCO + H_2$	3.00×10^{7}	2.0	10,000	[200]
227.	$CH_2CO + O \rightleftharpoons HCCO + OH$	2.00×10^{7}	2.0	10,000	[200]
228.	$CH_2CO + OH \rightleftharpoons CH_2OH + CO$	1.01×10^{12}	0.0	−1,013	[76,237]
229.	$CH_2CO + OH \rightleftharpoons CH_3 + CO_2$	6.74×10^{11}	0.0	−1,013	[76,237]

Parameters for use in the modified Arrhenius expression $k = AT^{\beta} \exp(-E/[RT])$.
Units are mol, cm, s, cal.
[a] Expressed as the sum of the rate constants.
[b] Enhanced third-body efficiencies: Ar = 0.7, H_2 = 2, H_2O = 6, CH_4 = 3, CO = 1.5, CO_2 = 2, C_2H_6 = 3.
[c] The expression of $k_{115,0}$ is valid for 600–3000 K. Zhu et al. [177] have also provided an expression for 200–500 K.
[d] Enhanced third-body efficiencies: H_2 = 2, H_2O = 5, CO = 2, CO_2 = 3.
[e] Enhanced third-body efficiencies: H_2O = 5.
[f] Troe parameters fitted to $F_{\text{cent},190} = 0.601T^{-0.162} \exp\left(\frac{-1.07}{RT}\right)$ [226].
[g] Estimate based on $k_{CH_3CHO+OH\rightarrow\text{prod.}}$ [228] and branching ratios [229].

characterized, whereas measurements of $C_2H_6 + HO_2$ (R97) and $C_2H_6 + O_2$ (R98) are few and generally of an earlier date. For the reaction of C_2H_6 with O atoms (R95), the direct measurements of Mahmoud et al. [129] were preferred.

The C_2H_5 radical is typically consumed by thermal dissociation or by reaction with O_2. The dissociation reaction is well characterized experimentally in the reverse direction (R112) [76]. The reaction is near the high-pressure limit at room temperature and ambient pressure, while it is well within the falloff region at 800 K. The experimental studies mostly used He as bath gas, but comparisons with experiments in N_2 in the falloff region [130,131] indicate no appreciable differences between He and N_2 as collision partner.

Miller and coworkers [132,133] recently conducted a master equation analysis of the reaction between C_2H_5 and O_2. Below 575 K, the reaction is dependent on pressure and temperature in a way that is typical for adduct formation (R106), i.e., high pressure and/or low temperatures favoring stabilization of the adduct, whereas concentrations of the bimolecular products increase when the conditions shift toward low pressure and/or high temperatures. Between 575 and 750 K, the reaction enters a transition region where the rate constant exhibits a biexponential decay to become equivalent with the low-pressure limit at 750 K regardless of the system pressure. The direct elimination of HO_2 (R107) from the adduct $C_2H_5OO^*$ is the energetically favorable route among potential bimolecular product channels. The ratio $k_{107}/(k_{106} + k_{107})$ increases toward unity within this temperature span, and at temperatures above 750 K the reaction has effectively become bimolecular with no appreciable formation of C_2H_5OO. In addition, the rate constant has become independent of pressure and only weakly dependent of temperature. Miller and Klippenstein [133] fitted the theoretical model to Arrhenius expressions for the three

elementary reactions: $C_2H_5 + O_2 \rightleftharpoons C_2H_5OO$ (R106), $C_2H_5 + O_2 \rightleftharpoons C_2H_4 + HO_2$ (R107), and $C_2H_5OO \rightleftharpoons C_2H_4 + HO_2$ (R129). The reaction (R129) is still in the falloff region at 100 bar and temperatures >700 K, which are conditions relevant to the present study. The present mechanism includes the pressure-dependent rate expressions of (R106) and (R129), whereas the rate constant for (R107) is simplified as $k_{107,0}$.

Under the conditions of the present work, also radical–radical reactions involving C_2H_5 become important, particularly that of C_2H_5 with HO_2. This reaction forms an energized $C_2H_5OOH^*$ adduct that either decomposes to $C_2H_5O + OH$ (R105) or via an H-atom transfer to $C_2H_4 + H_2O_2$ or $C_2H_6 + O_2$ (–R98). In the present mechanism, the overall rate constant and dominant product channel (R105) were adopted from Ludwig et al. [134]. However, these data are not consistent with earlier results [135], and more work is desirable. The reaction with atomic hydrogen can proceed via association, followed by either stabilization of C_2H_6 (R100) or dissociation to $CH_3 + CH_3$ (–R15); or through a direct abstraction mechanism yielding $C_2H_4 + H_2$. The rate expression for (R100) is drawn from the GRI-Mech 3.0 release [136]; it is in reasonable agreement with the theoretical work of Harding and Klippenstein [137]. This channel is expected to dominate over the direct abstraction channel. The reaction between C_2H_5 and O atoms has a number of potential product channels, e.g. $CH_3 + CH_2O$ (R101), $CH_3CHO + H$ (R102), $C_2H_4 + OH$ (R103), $CO + CH_4 + H$, and $CO + CH_3 + H_2$. We have adopted the rate constants from Slagle et al. [138]. The product yields were supported by Hoyermann et al. [139], but are still in discussion [140,141]. Only a room temperature measurement of $C_2H_5 + OH$ (R104, –R163) has been reported [142], and the rate constants for the two channels are estimates [106,143].

Formation of ethylperoxides is promoted by the high pressure and low temperatures of the present study. In the absence of measurements, rate constants for reactions of C_2H_5OO and C_2H_5OOH are estimates based on analogies between C_1 and C_2-peroxy reactions. In most cases, this is expected to be a reasonable assumption considering the similarities of bond dissociation energies. Hence, $D_{298}(C_2H_5OO{-}H) = 84.8 \pm 2.2$ kcal/mol [67] is within range of $D_{298}(CH_3OO{-}H) = 87.8 \pm 1.0$ kcal/mol [67], and $D_{298}(C_2H_5O{-}OH) = 45.2$ kcal/mol compares reasonably well with $D_{298}(CH_3O{-}OH) = 42.6 \pm 1$ kcal/mol [66].

At the temperatures of the present study, C_2H_5OOH is consumed mainly by thermal dissociation (R146). The rate constant is assumed to be similar to that for CH_3OOH (R32); this value agrees within a factor of 2 with the only available measurement for k_{146} [144]. The reaction with HO_2 (R134) is one of the few elementary reactions from the C_2H_5OO subset that has been investigated experimentally [145–149], with all measurements conducted at low temperatures (210–480 K). The rate constant is taken from the evaluation by Tyndall et al. [108]. Experimental observations [150–152] indicate that the direct abstraction channel to $C_2H_5OOH + O_2$ (R134) dominates at room temperature. According to the recent ab initio calculations of Hou et al. [153], other product channels, in particular $CH_3CHO + OH + HO_2$, become competitive at higher temperatures, but these are not included in the present mechanism. It should be noted that k_{134} lies 50%–60% above the rate constant of the analogue reaction between CH_3OO and HO_2 at 298–500 K. This agrees with the expectation that the rate constants of $RO_2 + HO_2$ increase with increasing size of R [149].

There are a significant number of measurements of the self-reaction of C_2H_5OO to $C_2H_5O + C_2H_5O + O_2$ (R144) and $CH_3CHO + C_2H_5OH + O_2$ (R145) [145,147,154–161]. These all fall in the low-temperature range from 218 to 490 K. The room temperature measurements of the overall rate constant are generally in good agreement, but there are some controversy regarding the temperature dependence. The values of k_{145} and k_{144} in Table III are fitted expressions based on $k_{144} + k_{145}$ from Fenter et al. [147] and data for the branching fraction from Lightfoot et al. [162].

The thermal dissociation of C_2H_5O proceeds either through scission of the C—C bond to yield $CH_3 + CH_2O$ (R156), or by elimination of one of the secondary H atoms to form $CH_3CHO + H$ (R157). Within recent years, a number of studies of the thermal decomposition of C_2H_5O have been published [118,163–167] as well as some reviews [168–170]. Among these, Caralp et al. [165] conducted the only experimental investigation of the complete falloff curves at total pressures between 0.001 and 60 bar and temperatures from 391 to 471 K, and we have adopted the value of k_{156} from this study. Owing to the dominance of the C—C bond dissociation channel at low temperatures, recent studies of the alternative channel to $CH_3CHO + H$ (R157) have all been theoretical and concerned with the limiting rate constant at high pressure [118,165–167,171]. The proposed expressions of $k_{157,\infty}$ show significant scatter when extrapolated toward high temperatures. Again, the preferred rate expression is taken from Caralp et al. [165]. In the absence of data for the low-pressure limit of (R157), this reaction is only represented by the high-pressure limit in the present mechanism.

Direct measurements of $C_2H_5O + O_2$ (R160) [172–174], as well as relative rate measurements [175], and

recent ab initio results [176] are all in good agreement but cover only the low-temperature range <500 K. The preferred rate expression is drawn from the most recent work [174]. The abstraction reactions between C_2H_5O and H (R158), and OH (R159), are expected to be fast and proceed with little or no energy barrier.

The most important consumption step for C_2H_4 under the present conditions is reaction with OH. The recent ab initio study by Zhu et al. [177] identified three important product channels, 2-C_2H_4OH (hydroxyethyl) (R115), $H + H_2CCHOH$ (ethenol) (R116), and $C_2H_3 + H_2O$ (R117). Their calculations indicate that at atmospheric pressure and temperatures <500 K, the reaction almost exclusively proceeds via (R115) to form 2-C_2H_4OH with a slight negative temperature dependence. This is in good agreement with experiments [178–180]. At temperatures roughly between 800 and 1000 K, both bimolecular channels, (R116) and (R117), become competitive. The rate constant governing the path to $C_2H_3 + H_2O$ shows a strong positive temperature dependence, which makes (R117) the predominant reaction channel >1000 K.

For the abstraction channel of $C_2H_4 + H$ (R111), we have adopted the rate constant from the Baulch evaluation [76]. For $C_2H_4 + O$ we prefer the overall rate constant from Klemm et al. [181], with the branching fraction for the different product channels (R113, R114) chosen as a mean value between literature data [182–187]. Experimental characterization of the reaction $C_2H_4 + HO_2$ is limited to the relative rate measurements by Baldwin et al. [188–190] at 673–773 K. In the present mechanism, the reaction is represented by the product channels to $C_2H_5 + O_2$ (–R107) and C_2H_5OO (–R129), both listed in the reverse direction. However, the value for k_{-129} does not comply with an expected activation energy barrier for the reaction of 8.4–12.1 kcal/mol [132,191,192]. The experimentally based activation energy for $C_2H_4 + HO_2 \rightleftharpoons C_2H_4O + OH$ from Baldwin et al. [190] is substantially higher than the calculated energy barrier for the initial rate determining association step of $C_2H_4 + HO_2$. Additional experimental investigations of this complex reaction are desirable.

There are no measurements of the initiation reaction of C_2H_4 with molecular oxygen (R118,R119). Benson [193] proposed a reaction mechanism involving initial association with the biradical adduct $CH_2CH_2OO^*$ that may dissociate to yield vinoxy radicals (R118) or formaldehyde (R119). From thermochemical considerations, Benson estimated that both pathways contribute actively to the product formation, with the initial adduct formation step with an activation energy of about 39 kcal/mol being rate determining. This value is substantially lower than the activation energy of the alternative direct abstraction reaction to $C_2H_3 + HO_2$. In the present work, we have assumed the temperature-dependent preexponential factor to be similar to that of the reaction between C_2H_2 and O_2 [193] together with an activation energy of 39 kcal mol and an assumed branching fraction of $k_{118}/k_{119} = 1$.

The subsets for C_2H_3, CH_3CHO, CH_3CO, CH_2CHO, and CH_2CO were mostly collected from literature evaluations [76,106], whereas reactions involving ethanol (C_2H_5OH) and the two alkyl radical derivatives 1- and 2-hydroxyethyl (1-C_2H_4OH and 2-C_2H_4OH) were drawn from Marinov [143]. The vinyl radical (C_2H_3) is an important intermediate in combustion processes operated at high temperatures, but it is not expected to play a significant role in the present study. The large bond dissociation energy of $CH_2CH{-}H$ ($D_{298} = 110.6$ kcal/mol [194]) causes H-abstraction from C_2H_4 to be quite energy intensive and C_2H_4 is largely converted to other products.

RESULTS AND DISCUSSION

CH_4/O_2 Experiments

Mixtures of CH_4 and O_2 highly diluted in N_2 were reacted at three different pressures: 100, 90, and 50 bar, and different stoichiometric ratios representing reducing ($25 < \phi < 99$), stoichiometric ($\phi \approx 1$), and oxidizing conditions ($\phi \approx 0.04$). No recognizable conversion was observed at 50 bar and stoichiometric conditions. The experimental conditions are summarized in Table IV. τ denotes the temperature-dependent residence time in the isothermal section of the reactor. The diluted conditions ensured a low heat release during the reaction, and calculations of the adiabatic temperature rise gave values <26 K for all experiments. The carbon balances closed within 6% in all the experiments with CH_4/O_2. The experimental data were obtained as mole fractions as a function of the reactor temperature from 600 to 900 K using intervals of 25 K. The lower bound of the temperature interval (600 K) was well below the temperature where reactant conversion initiated. Measurements include concentration profiles of CH_4, O_2, CO, and CO_2 for all experiments. In addition, measurements of C_2H_6, C_2H_4, and CH_3OH are presented for the reducing experiments A–D. These species were also observed during the stoichiometric experiments, but in too low concentrations to facilitate a reliable model validation. Likewise, C_2H_5OH was only observed in trace amounts. At the oxidizing conditions, only CO and CO_2 were observed as products. The numerical predictions of the concentration profiles were obtained from (isothermal) plug flow simulations

Table IV Reaction Conditions Applied During Experiments with CH_4/O_2

	Reactant Concentrations					
Experimental ID	CH_4 (ppm)	O_2 (ppm)	Pressure (bar)	Temperature (K)	ϕ^a	τ (s K)
A	4.63%	936	100	598–898	98.8	12070/T
B	4.42%	1,940	100	598–898	45.6	11690/T
C	1.12%	889	90	598–898	25.2	10450/T
D	4.66%	976	50	598–898	95.5	5870/T
E	1,587	2,903	100	673–898	1.09	11870/T
F	1,491	2,888	90	598–898	1.03	10430/T
G	964	4.57%	100	648–898	0.042	12020/T
H	993	5.00%	90	598–898	0.040	10740/T
I	968	4.60%	50	648–898	0.042	6030/T

Concentrations are in ppm if otherwise not stated.

The reactant concentrations are balanced by N_2.

The volumetric flow rate was ~3 SLPM in all experiments. The exact flow rates are incorporated in the expressions of the temperature dependent residence times $\tau(T)$.

[a] Stoichiometric ratio (ϕ) is based on $CH_4 + 2O_2 \rightarrow CO_2 + 2H_2O$.

using the SENKIN code [195] from the CHEMKIN-II library [82]. Modeling predictions are not sensitive to reactions occurring in the heating and cooling sections of the reactor.

Initial modeling results indicated a premature fuel ignition of 25–50 K under all the experimental conditions compared to the measured concentration profiles. The offset was dependent on the absolute hydrocarbon concentration and was most severe under reducing conditions. Figure 2 shows a first-order sensitivity analysis with respect to CH_4 at temperatures just above the initiation temperature for the stoichiometric conditions at 100 bar. The principal initiation reaction in the chemical system at hand is $CH_4 + O_2 \rightleftharpoons CH_3 + HO_2$ (–R13), but the calculated initiation temperature is not sensitive to the initiation step. Rather, the predicted temperature for onset of reaction depends on the generation of chain carriers at early reaction times, showing positive sensitivity coefficients to reactions leading to CH_3O that may subsequently dissociate to form atomic hydrogen, and negative values to a number of steps that are in effect chain terminating. While adjustment of the rate constant for any of these reactions may improve the prediction of the initiation temperature, there are also issues related to the experimental conditions, such as loss of radical species at the reactor wall. Deactivation of radical species is of particular concern in laboratory reactors that typically exhibit large surface-to-volume ratios. The applied reactor material is quartz, which is considered to be comparatively inert. Experiments [196] and theoretical investigations [197] have, nonetheless, indicated that even quartz may exhibit a

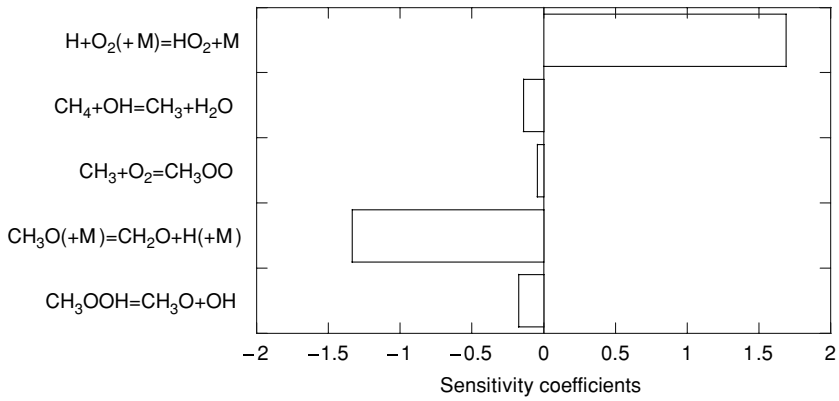

Figure 2 First-order sensitivity coefficients for the most important elementary reactions with respect to initiation, i.e. the predicted concentration of CH_4 for conditions corresponding to set E (100 bar, $\phi = 1.09$) at a temperature just above the initiation temperature.

minor reactivity toward hydrocarbon oxidation at high pressure.

It is difficult to quantify the extent of surface activity in the present work based on the available measurements. As mentioned above, radical deactivation seems to increase with increasing CH_4 concentrations. Modeling predictions identify CH_3OO consumption as an important bottleneck in the low-temperature ignition of CH_4 at high pressures. In a previous modeling study of rich CH_4/O_2 mixtures at >50 bar and 600–800 K, Vedeneev et al. [198] included deactivation of CH_3OO radicals on the reactor wall,

$$CH_3OO \xrightarrow{\text{wall}} \text{inert} \qquad (R_{\text{surf}})$$

Following Vedeneev et al., we have chosen to include R_{surf} to improve the prediction of the temperature for onset of reaction. Different rate constants was employed under reducing conditions ($k_{\text{surf}} = 45\ \text{s}^{-1}$) and stoichiometric/oxidizing conditions ($k_{\text{surf}} = 9.5\ \text{s}^{-1}$), but for simplicity any pressure dependence was neglected. In effect, the introduction of this surface reaction adjusts the initiation time in the system. Calculations show that the conversion of reactants after initiation exhibits little sensitivity to surface removal of CH_3OO. If similar deactivation reactions were introduced for other hydrocarbon radicals, such as CH_3 and CH_3O, they would give rise to markedly different behaviors in the fuel conversion compared to experiments.

Figures 3 and 4 compare experimental and modeling results at reducing conditions, whereas data sets obtained at stoichiometric and oxidizing conditions are presented in Figs. 5 and 6, respectively. With the inclusion of R_{surf}, simulations of the major species CH_4, O_2, CO, and CO_2 are everywhere in very good agreement with the experimental concentration profiles. It is noteworthy that in the reducing experiment D at 50 bar (Fig. 4), there is a region above 800 K with a negative temperature coefficient, indicated by an increase in $[O_2]$ with the temperature. The model captures this feature well. A net rate analysis indicates that this phenomenon can be attributed to a significant buildup of CH_3 and HO_2 radicals that drives the reaction $CH_3 + HO_2 \rightleftharpoons CH_4 + O_2$ (R13) toward the original fuel and oxidizer. The phenomenon is not observed in the other reducing experiments, but in the stoichiometric experiments shown in Fig. 5, the net conversion rate of CH_4 (and O_2) tends to slow down above ~800 K.

Predictions of CH_3OH at reducing conditions in Fig. 3 (right) and Fig. 4 (right) are generally

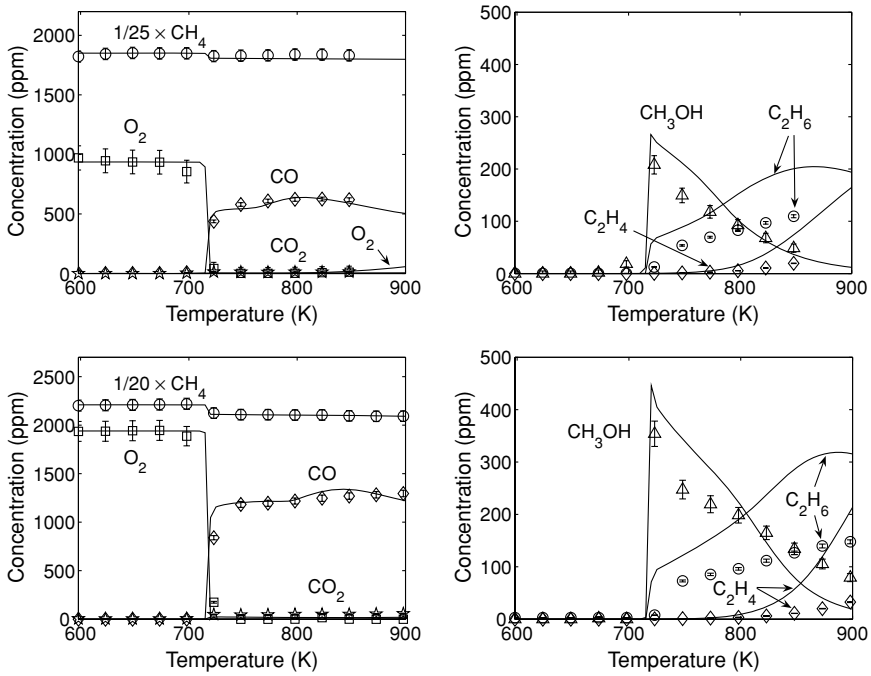

Figure 3 Results of reducing experiments with CH_4/O_2. Concentration profiles are shown as a function of the reactor temperature. Top: Experiment A (100 bar, $\phi = 98.8$). Bottom: Experiment B (100 bar, $\phi = 45.6$). Reaction conditions are provided in Table IV. Symbols mark experimental results. Lines denote model predictions obtained at isothermal conditions. Measuring uncertainties are ±2.6% for $CO/CH_4/C_2H_4/C_2H_6$, ±5.3% for O_2, ±4.3% or ±3 ppm for CO_2, and ±6.0% or ±3 ppm for CH_3OH.

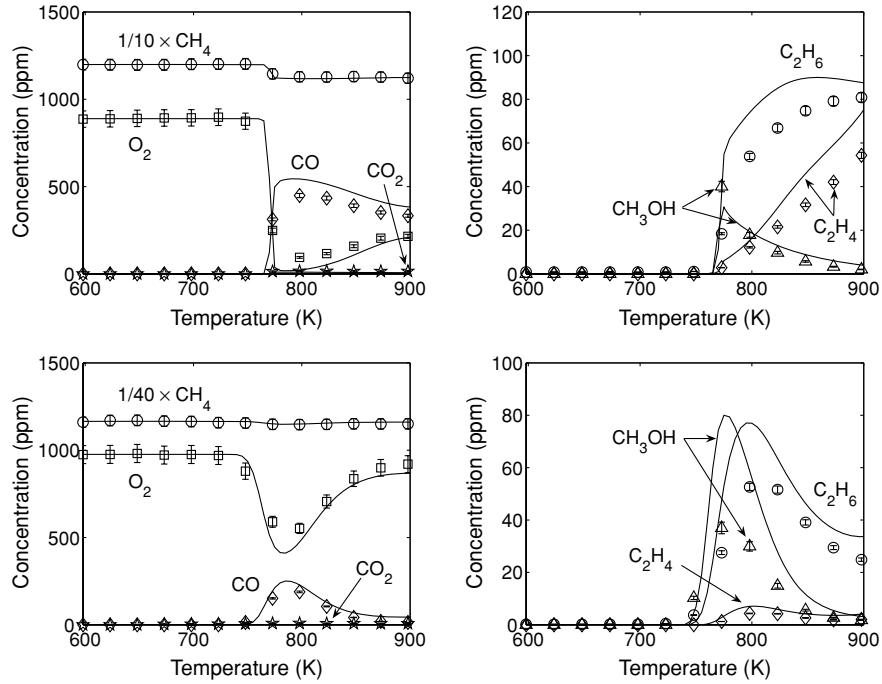

Figure 4 Results of reducing experiments with CH_4/O_2. Concentration profiles are shown as a function of the reactor temperature. Top: Experiment C (90 bar, $\phi = 25.2$). Bottom: Experiment D (50 bar, $\phi = 95.5$). Reaction conditions are provided in Table IV. Symbols mark experimental results. Lines denote model predictions obtained at isothermal conditions. See caption of Fig. 3 for measuring uncertainties.

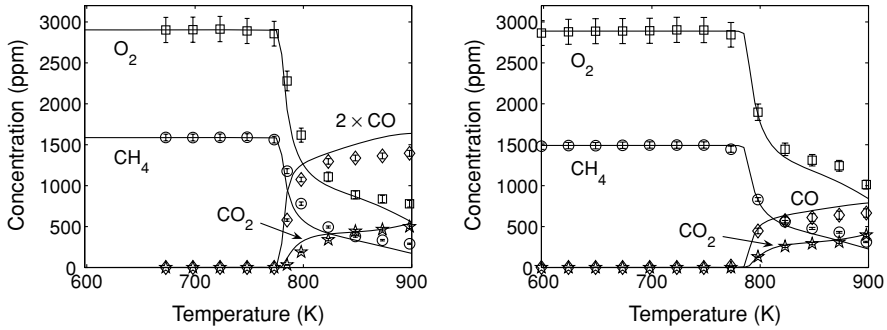

Figure 5 Results of stoichiometric experiments with CH_4/O_2. Concentration profiles are shown as a function of the reactor temperature. Left: Experiment E (100 bar, $\phi = 1.09$). Right: Experiment F (90 bar, $\phi = 1.03$). Reaction conditions are provided in Table IV. Symbols mark experimental results. Lines denote model predictions obtained at isothermal conditions. Measuring uncertainties are $\pm 2.6\%$ for CO/CH_4, $\pm 5.3\%$ for O_2, and $\pm 4.3\%$ or ± 3 ppm for CO_2.

satisfactory. A substantially higher concentration of CH_3OH is observed at 100 bar than at 50 bar, which suggests that pressure has a promoting effect. The only significant deviation between experiments and modeling results is observed at 50 bar (Fig. 4, bottom right), where the measured peak concentration of CH_3OH is overpredicted by roughly a factor of 2. However, the present calculations of the CH_3OH concentration are very sensitive to the magnitude of the fuel conversion and even minor discrepancies between measured and calculated concentrations of CH_4 (and O_2) may have a substantial impact on the formation of CH_3OH. Conceivably, the overprediction of the peak in CH_3OH may be attributed to a minor overprediction of the reactant conversion, rather than an erroneous description of the CH_3OH formation mechanism.

Simulations of C_2H_6 and C_2H_4 are satisfactory to the point that the main trends are reproduced by the model. However, the model overpredicts the measured concentration by up to a factor of 2 during the reducing 100 bar experiment in Fig. 3 (right), whereas the discrepancies are less pronounced during the

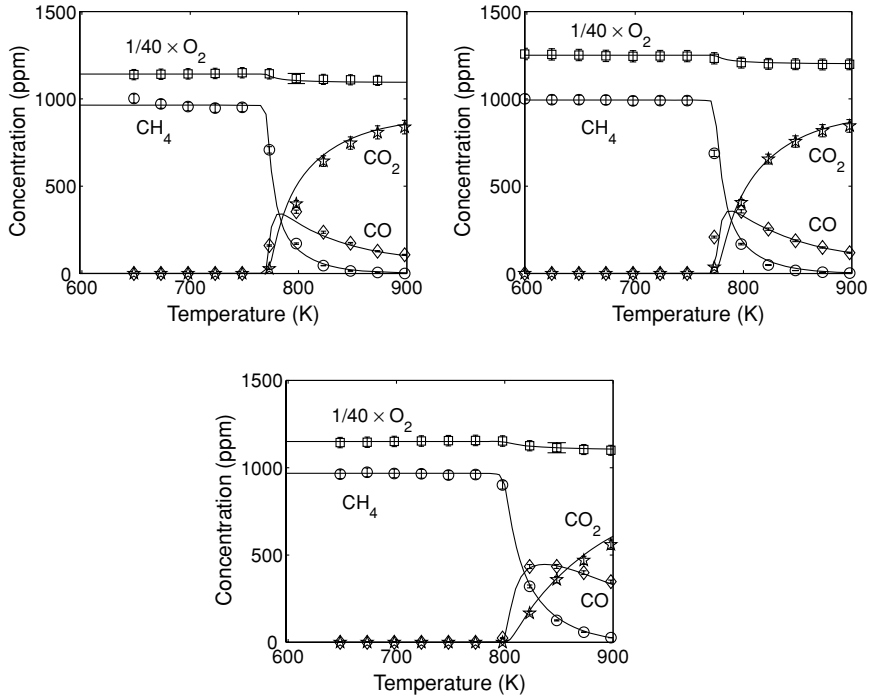

Figure 6 Results of oxidizing experiments with CH_4/O_2. Concentration profiles are shown as a function of the reactor temperature. Top left: Experiment J (100 bar, $\phi = 0.042$). Top right: Experiment G (90 bar, $\phi = 0.040$). Bottom: Experiment L (50 bar, $\phi = 0.042$). Reaction conditions are provided in Table IV. Symbols mark experimental results. Lines denote model predictions obtained at isothermal conditions. Measuring uncertainties are $\pm 2.6\%$ for $O_2/CO/CH_4$, and $\pm 4.3\%$ or ± 3 ppm for CO_2.

corresponding experiments at 90 and 50 bar in Fig. 4 (right). Figure 7 shows a first-order sensitivity analysis with respect to C_2H_6 for the reducing conditions at 100 bar and at 800 K. The analysis confirms the importance of the CH_4 consumption reactions (R1, R2, R3), as well as the self-association reaction of CH_3 radicals (R14), which is the main route to C_2H_6 under the investigated conditions. At 100 bar and 800–900 K, the value of k_{14} is within 10% of the high-pressure limit. As discussed above, the temperature dependence of the high-pressure limit is still in question; Baulch et al. [76] assigned an uncertainty factor of 2 to $k_{14,\infty}$ at 300–1000 K. The predicted C_2H_6 concentration is also sensitive to the size and composition of the O/H radical pool. Reactions like $H + O_2 \rightarrow O + OH$ and dissociation of CH_3O to $CH_2O + H$ show large negative

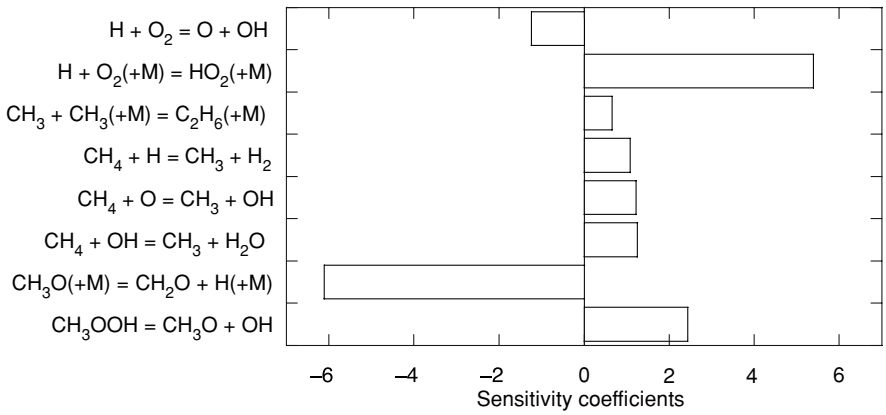

Figure 7 First-order sensitivity coefficients for the most important elementary reactions with respect to formation of C_2H_6 for conditions corresponding to set A (100 bar, $\phi = 98.8$) at 800 K.

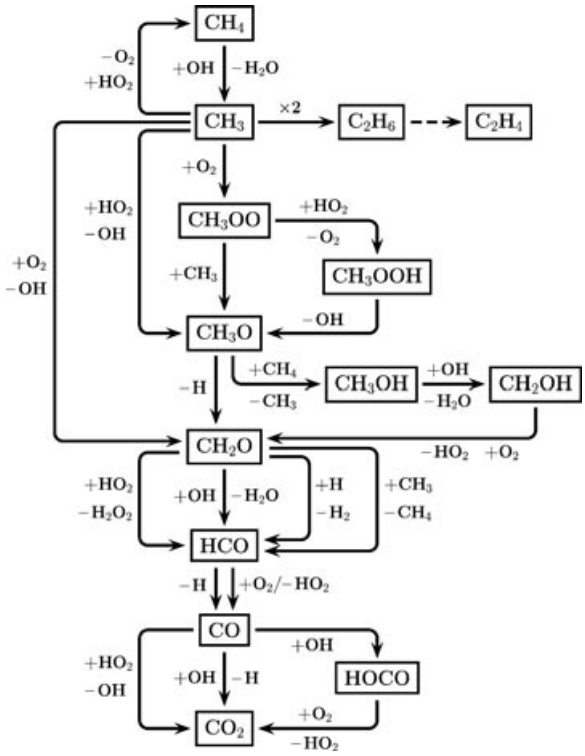

Figure 8 Main reaction pathways for CH_4 conversion at the investigated conditions of experiment A–I. The fractional contributions of competing pathways are dependent on the reaction conditions (see text). The dashed line denotes a more complex underlying mechanism that will be considered in details in a later section of this paper.

sensitivity coefficients, whereas formation of HO_2 through recombination of H with O_2 has a positive value. This indicates that chain-branching reactions limit the C_1 to C_2 conversion under these conditions.

Figure 8 provides an overview of the most important pathways involved in the oxidation of CH_4 at high pressure, according to the model. The CH_4 is mostly consumed by reaction with OH (R3), independent of stoichiometry. When CH_4 is available in sufficient concentrations to make it a frequent collision partner, reaction with other radical species contribute to the consumption of CH_4. The most important of these reactions is $CH_3O + CH_4 \rightarrow CH_3OH + CH_3$ (R51), the major source of CH_3OH.

The OH radicals are mainly produced from thermal dissociation of H_2O_2, formed from $HO_2 + HO_2 \rightarrow H_2O_2 + O_2$. Formation of HO_2 radicals occurs mainly through recombination of H and O_2, promoted by the high pressure. At oxidizing conditions, also H-abstraction from hydrocarbon species by molecular oxygen, e.g. $HCO + O_2 \rightarrow CO + HO_2$ and $HOCO + O_2 \rightarrow CO_2 + HO_2$, contributes.

As indicated in Fig. 8, there is a number of important consumption steps for CH_3. High pressure and low temperatures facilitate reaction with molecular oxygen to CH_3OO (R9). This oxidation path is important roughly below 800 K, and it is further enhanced at oxidizing conditions where O_2 is readily available. However, as the temperature increases to 900 K, the branching ratio shifts toward the competing product channel $CH_3 + O_2 \rightarrow CH_2O + OH$ (R11) as a result of the comparatively low thermal stability of CH_3OO. Reaction (R9) is the only active pathway to CH_3OO, which means that the potential consumption of CH_3 through the subsequent reaction between $CH_3OO + CH_3$ (R22) is restrained by the carbon flux through (R9).

The reaction between $CH_3 + HO_2$ is important at all stoichiometries and pressures considered in the experimental work; most pronounced at stoichiometric and reducing conditions. The branching ratio between the two competing pathways to $CH_3O + OH$ (R12) and $CH_4 + O_2$ (R13) is ~3 at 800–900 K in favor of (R12), but under conditions with high CH_3 and HO_2 concentrations ($\phi \geq 1$) this is still sufficient to facilitate a substantial regeneration of $CH_4 + O_2$ via (R13), as observed in the experiments. At these conditions, CH_3 is also consumed by reactions with hydrocarbon species, most importantly the self-recombination reaction $CH_3 + CH_3(+M) \rightarrow C_2H_6(+M)$ (R14) and reaction with formaldehyde, $CH_2O + CH_3 \rightarrow HCO + CH_4$ (R84).

The CH_3OO radicals are converted to CH_3O, either directly through reaction with CH_3 (R22), or indirectly via formation of CH_3OOH (R20) and subsequent dissociation to $CH_3O + OH$ (R32), which is favored at $\phi < 1$. It is noticed that the latter path effectively yields a net result identical to $CH_3 + HO_2 \rightarrow CH_3O + OH$ (R12). Thermal dissociation (R42) is the main consumption step for CH_3O at the dilute conditions applied in the experimental work. Even so, the observed formation of CH_3OH in the experiments can be attributed to the competing reaction with CH_4 (R51). Oxidation of CH_3OH involves intermediate formation of CH_2OH; mainly via reaction with OH radicals (R59). The CH_2OH radicals are further oxidized to CH_2O by molecular oxygen (R70). Association of CH_2OH with CH_3 (–R162) is the main route to C_2H_5OH during conversion of C_1 fuels. This way formation of C_2H_5OH is restrained by the availability of CH_3OH, which is generally low at the present dilute conditions, and hence, explains why only trace amounts of C_2H_5OH were observed during the experiments with pure CH_4.

As indicated in Fig. 8, CH_2O can be oxidized through several channels, but most important are the reactions with OH (R81) and HO_2 (R82). The reactions with CH_3 (R84) and H atoms (R79) only

provide significant contributions at reducing conditions. The subsequent conversion of HCO to CO is mainly governed by thermal dissociation (R85) except at oxidizing conditions where H-abstraction by molecular oxygen (R91) becomes more important due to the high availability of O_2. CO is largely oxidized by reaction with OH radicals, either directly to CO_2 via CO + OH → CO_2 + H or through the sequence CO + OH → HOCO, HOCO + O_2 → CO_2 + HO_2. The CO + HO_2 reaction is only of minor importance under the present conditions.

CH_4/C_2H_6 Experiments

This section presents experiments with mixtures of CH_4 and C_2H_6, where C_2H_6 constitutes 10% of the hydrocarbon feed on a molar basis. This is a realistic composition compared to raw natural gas. The experiments involve pressures of 100 and 50 bar, and stoichiometric ratios comparable to those applied above for CH_4 oxidation. The experimental conditions are summarized in Table V. Calculations of the adiabatic temperature rise gave values <24 K for all experiments. Moreover, the carbon balances were satisfied within 5%. Measurements include concentration profiles of CH_4, C_2H_6, C_2H_4, O_2, CO, and CO_2 for all experiments. Moreover, data for CH_3OH and C_2H_5OH are presented for the reducing experiments, where the alcohols were formed in concentrations significantly above the detection limit.

The experimental and modeling results from the mixed CH_4/C_2H_6 experiments J–N are presented in Figs. 9–11. Simulations are conducted with the same rate constants for surface loss of CH_3OO as for the pure CH_4 experiments, while no surface deactivation of the analogue C_2H_5OO radical was included. There is generally a good agreement between experimental and calculated concentration profiles. In particular at reducing conditions, the simulations of all the measured compounds are satisfactory. The reducing experiment J at 100 bar (Fig. 9, left) is directly comparable with the pure CH_4 experiment B that was previously presented in Fig. 3 (bottom). These results show negligible differences in terms of the initiation temperature, but a slightly higher yield of alcohols, including a small contribution from C_2H_5OH, is obtained when C_2H_6 is present in the feed. However, significant uncertainties are attributed to the observations of higher alcohol yields, which makes it impossible to conclude whether C_2H_6 has a minor promoting effect or not.

In the stoichiometric and oxidizing experiments in Figs. 10 and 11, the model overpredicts the concentration of C_2H_4 that arises shortly after the fuel initiation temperature. Figure 12 shows a first-order sensitivity analysis with respect to C_2H_4 for conditions corresponding to set L (100 bar, $\phi = 0.936$) at 800 K. The results of the analysis indicate that the prediction of C_2H_4 is sensitive to reactions governing the size and composition of the radical pool, rather than formation and consumption reactions for ethylene. A number of the most sensitive reactions, in particular for peroxides, are associated with significant uncertainties, and more work on these steps is desirable to resolve the discrepancy.

The oxidation of C_2H_6 is governed by a reaction mechanism that involves C_2 hydrocarbon species and an underlying mechanism for C_1 hydrocarbons. The presence of 10% C_2H_6 in the hydrocarbon feed does not impose significant changes in the C_1 reaction mechanism (see Fig. 8), and it will therefore not be subjected to discussions in the following. Figure 13 provides an overview of the C_2 reaction network. There are a number of competing pathways whose individual contributions are very dependent on the reaction conditions.

Similar to CH_4, the C_2H_6 oxidation chain is mainly initiated by reaction with OH (R96). However, the reactions C_2H_6 + CH_3 (R99) and C_2H_6 + H (R94) may account for up to 20% of the initial C_2H_6 conversion at

Table V Reaction Conditions Applied During Experiments with $CH_4/C_2H_6/O_2$

	Reactant Concentrations						
Experimental ID	CH_4 (ppm)	C_2H_6 (ppm)	O_2 (ppm)	Pressure (bar)	Temperature (K)	ϕ^a	τ (s K)
J	3.56%	3,987	1,929	100	598–848	44.1	11680/T
K	3.53%	3,963	2,040	50	598–898	41.4	5920/T
L	916	99	2,328	100	598–898	0.936	11880/T
M	773	99	5.28%	100	598–898	0.036	11320/T
N	900	99	5.50%	50	6737–898	0.039	5940/T

Concentrations are in ppm if otherwise not stated.
See caption of Table IV for other specifications.
[a] Stoichiometric ratio (ϕ) is based on $\alpha CH_4 + \beta C_2H_6 + (2\alpha + 7/2\beta)\,O_2 \rightarrow (\alpha + 2\beta)\,CO_2 + (2\alpha + 3\beta)\,H_2O$.

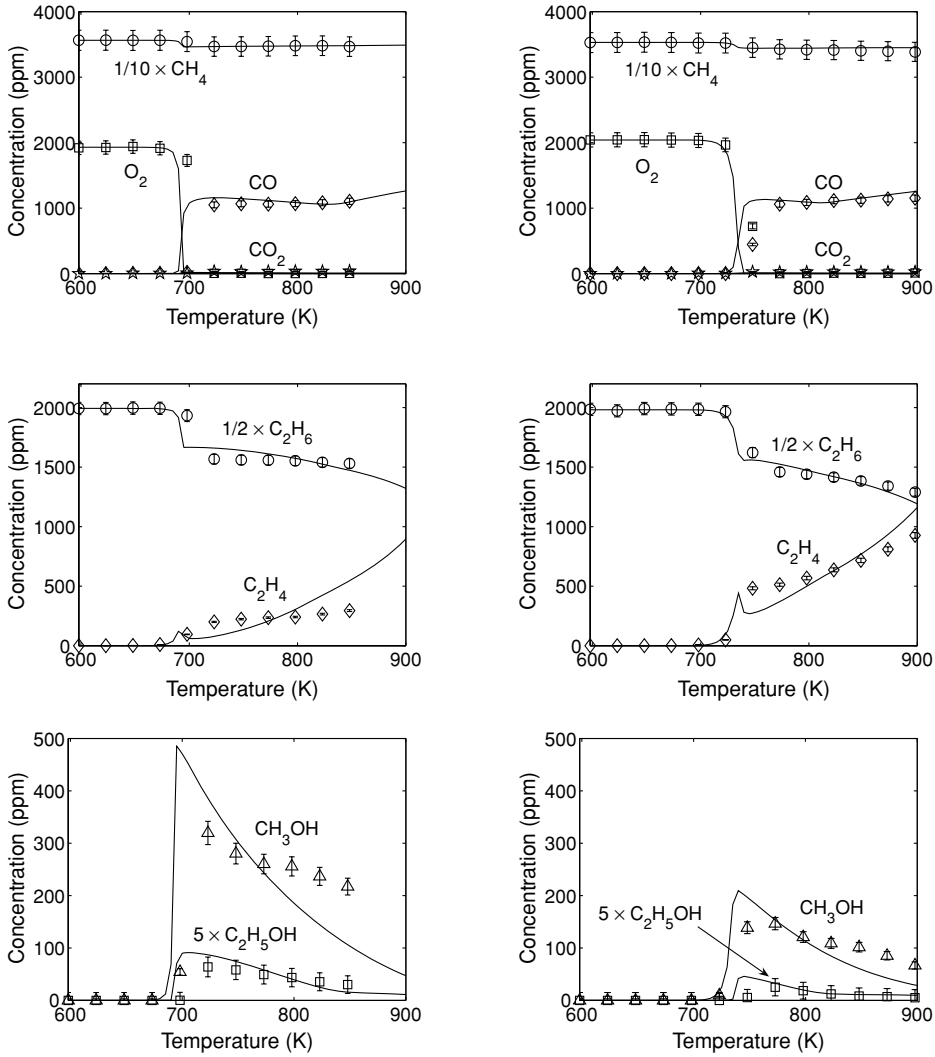

Figure 9 Results of reducing experiments with $CH_4/C_2H_6/O_2$. Concentration profiles are shown as a function of the reactor temperature. Left: Experiment J (100 bar, $\phi = 44.1$). Right: Experiment K (50 bar, $\phi = 41.4$). Reaction conditions are provided in Table V. Symbols mark experimental results. Lines denote model predictions obtained at isothermal conditions. Measuring uncertainties are ±4.3% for CO/CH_4, ±2.6% for C_2H_4/C_2H_6, ±5.3% for O_2, ±4.3% or ±3 ppm for CO_2, and ±6.0% or ±3 ppm for CH_3OH/C_2H_5OH.

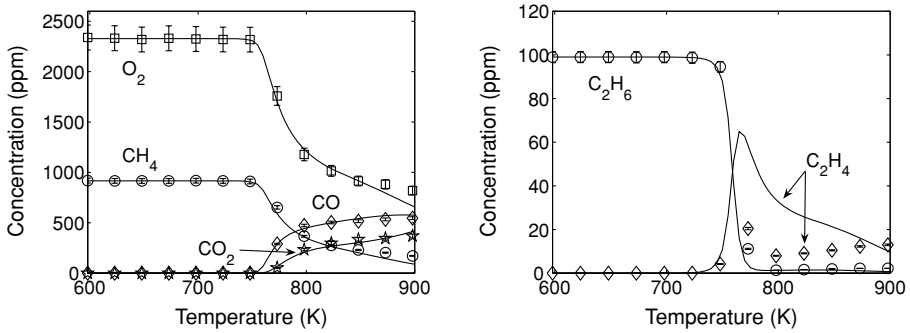

Figure 10 Results of stoichiometric experiment with $CH_4/C_2H_6/O_2$. Concentration profiles are shown as a function of the reactor temperature. Experiment O (100 bar, $\phi = 0.936$). Reaction conditions are provided in Table V. Symbols mark experimental results. Lines denote model predictions obtained at isothermal conditions. Measuring uncertainties are ±2.6% for $CO/CH_4/C_2H_4/C_2H_6$, ±5.3% for O_2, and ±4.3% or ±3 ppm for CO_2.

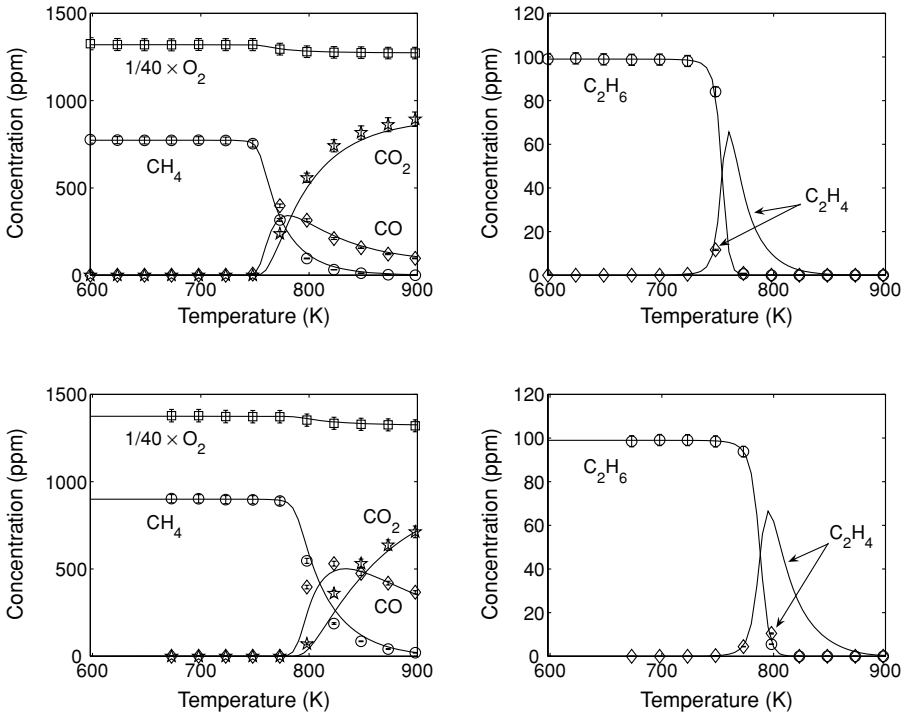

Figure 11 Results of oxidizing experiments with $CH_4/C_2H_6/O_2$. Concentration profiles are shown as a function of the reactor temperature. Top: Experiment M (100 bar, $\phi = 0.036$). Bottom: Experiment N (50 bar, $\phi = 0.039$). Reaction conditions are provided in Table V. Symbols mark experimental results. Lines denote model predictions obtained at isothermal conditions. Measuring uncertainties are ±2.6% for $O_2/CO/CH_4/C_2H_4/C_2H_6$, and ±4.3% or ±3 ppm for CO_2.

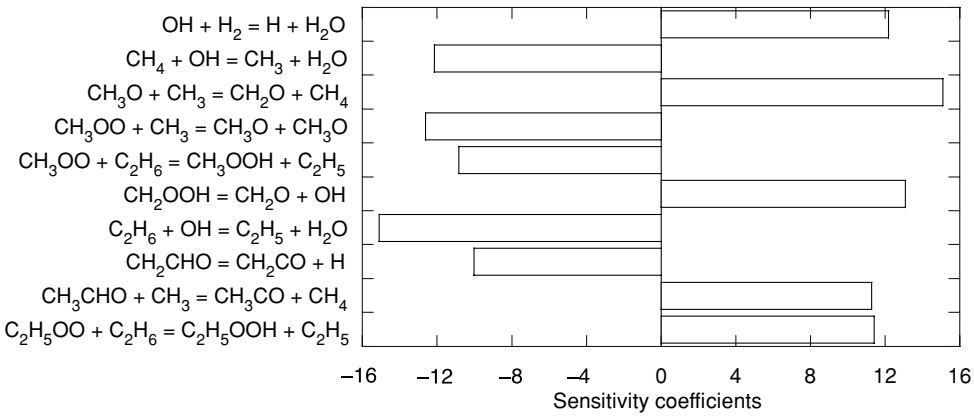

Figure 12 First-order sensitivity coefficients for the most important elementary reactions with respect to formation of C_2H_4 for conditions corresponding to set L (100 bar, $\phi = 0.936$) at 800 K.

$\phi \gg 1$. Association of CH_3 radicals (R14) provides a minor contribution to the C_2H_6 concentration at $\phi > 1$.

The C_2H_5 radical also shares similarities with the analogue CH_3 radical in terms of preferred reaction channels. At $\phi \leq 1$, the main reactant is molecular oxygen that either yields C_2H_5OO (R106) or $C_2H_4 + HO_2$ (R107). The branching ratio R106/R107 changes markedly across the investigated temperature range. Thus, formation of C_2H_5OO is favored by high pressure and low temperatures (<750 K), whereas (R107) dominates at higher temperatures regardless of the pressure. In the stoichiometric and oxidizing experiments, the fuel initiation temperature is close to 750 K, which means that C_2H_5 is almost completely converted to C_2H_4 via (R107). However, in the reducing experiments, the intermediate formation of C_2H_5OO gains substantial importance during the low-temperature conversion of the fuels.

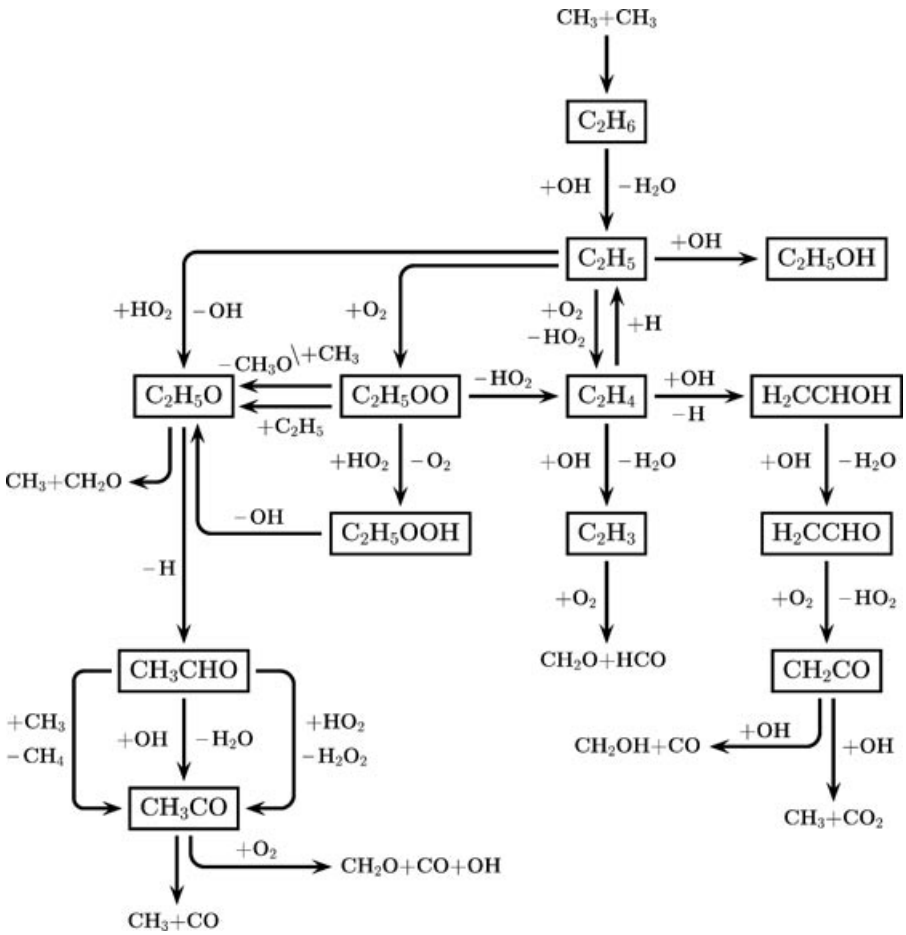

Figure 13 Main reaction pathways for C_2H_6 conversion at the investigated conditions of experiment J–N. The fractional contributions of competing pathways are dependent on the reaction conditions (see text). The mechanism of CH_4 conversion from Fig. 8 underlies the current reaction network. The reader may notice a number of similarities between these mechanisms.

The peroxyl radical C_2H_5OO is converted to C_2H_5O, either by reaction with CH_3 (R136) or C_2H_5 (R140) or indirectly through intermediate formation of C_2H_5OOH by H-abstraction from HO_2 (R134) and subsequent dissociation to $C_2H_5O + OH$ (R146). This mechanism is equivalent to the conversion of CH_3OO, as illustrated in Fig. 8. A small yield of $C_2H_4 + HO_2$ may arise from dissociation of C_2H_5OO (R129). This channel becomes more important at higher temperatures, but here, the concentrations of C_2H_5OO are typically low because of the shift in the branching ratio of $C_2H_5 + O_2$, which means that (R129), in practice, gains little importance during the conducted experiments.

The reaction $C_2H_5 + O_2 \rightarrow C_2H_4 + HO_2$ (R107) accounts for >90% of the formation of C_2H_4 at all investigated conditions. A substantial fraction may be converted back to C_2H_5 through association with H atoms (R112), whereas reactions with OH according to the present calculations lead to C_2H_3 (R117) and H_2CCHOH (R116) in comparable yields. The current model description of the oxidation of C_2H_4 by OH was taken from the theoretical work of Zhu et al. [177]. The reaction displays a complicated temperature and pressure dependence that was not treated in detail by Zhu et al., and updates of the current mechanism should consider the recent work of Senosiain et al. [199].

The reaction between C_2H_5 and HO_2 is mainly important at reducing conditions, where it competes with $C_2H_5 + O_2$. Regeneration of $C_2H_6 + O_2$ is negligible, so the only significant products are $C_2H_5O + OH$ (R105). This is different from the CH_4 mechanism where a considerable fraction of the CH_4 and O_2 is regenerated through the analogue reaction $CH_3 + HO_2 \rightarrow CH_4 + O_2$ (R13). A minor fraction of the C_2H_5 radical pool may be converted directly to C_2H_5OH by addition of OH radicals (–R163). At the applied experimental conditions, this is the main route to C_2H_5OH at temperatures >850 K, whereas the association of $CH_2OH + CH_3$ (–R162) predominates at lower temperatures.

The conversion of C_2H_5O takes place through thermal dissociation to $CH_3 + CH_2O$ (R156) and $CH_3CHO + H$ (R157), where the former channel accounts for >75% of the overall consumption of C_2H_5O at all the investigated conditions. The minor fraction that yields CH_3CHO may undergo further oxidation to CH_3CO through different reaction channels. The main reactants are OH (R195) and HO_2 (R198), while reaction with CH_3 (R200) only becomes important at reducing conditions. The CH_3CO radical is rapidly converted to C_1 products through C—C bond cleavage either facilitated by reaction with molecular oxygen (R211) or by thermal dissociation (R202).

As indicated in Fig. 13, there are several channels that convert C_2 to C_1 species. At oxidizing and stoichiometric conditions, this happens through addition/elimination reactions of $C_2H_3 + O_2$ (R126) and/or $CH_2CO + OH$ (R228, R229). At reducing conditions, decomposition of C_2H_5O (R156) and CH_3CO (R202, R211) constitutes the main pathways to the C_1 network.

CONCLUSIONS

A detailed chemical kinetic model for homogeneous combustion of the light hydrocarbon fuels CH_4 and C_2H_6 in the intermediate temperatures range, roughly 500–1100 K, and pressures up to 100 bar, has been developed and verified by experiments. Rate constants have been obtained from critical reviews of data for individual elementary reactions reported in the literature with particular emphasis on the conditions relevant to the present work. The kinetic model represents the current status of combustion kinetic research, but even so, this work has demonstrated that improved characterization is needed for a number of elementary reactions relevant to hydrocarbon oxidation chemistry; in particular reactions involving alkylperoxy species, e.g. CH_3OO, CH_3OOH, C_2H_5OO, end C_2H_5OOH. The experiments involved CH_4/O_2 and $CH_4/C_2H_6/O_2$ mixtures diluted in N_2, and were carried out in a high-pressure flow reactor at 600–900 K, 50–100 bar, and various reaction stoichiometries ranging from highly lean to fuel-rich conditions. Model predictions are generally satisfactory. The governing reaction mechanisms are outlined based on calculations with the kinetic model.

APPENDIX

During review, it was suggested that the kinetic model was tested against a broader range of experimental data. We have selected experimental data from shock tubes, laminar flames, and flow reactors for comparison with modeling predictions, but a comprehensive validation is outside the scope of the present work. Since the mechanism was developed for a low-temperature application, this required the addition of a number of species and reactions. The added subsets, most importantly reactions of singlet and triplet methylene, were drawn from previous modeling work [200]. The full mechanism is available as supplementary material or can be obtained from the authors. Other than adding subsets, no changes were made to the mechanism.

There has been numerous studies of methane ignition and there are some variation between results by different researchers. However, most of the published work appear to agree within a factor of 2 [201]. We have chosen the experimental data of Lifshitz et al. [14] on ignition delays in methane–oxygen–argon mixtures as test data for the model. These data cover temperatures from approximately 1600–2000 K and stoichiometries from 0.5 to 2.0, while pressure ranges from 2 to 13 atm. Figure A1 shows comparison between the experimental data and our calculations.

The ignition delay period can be divided into two subperiods [202]. The first subperiod, reaction initiation, involves initial formation of radicals, either by decomposition of the fuel molecule, $CH_4(+M) \rightarrow CH_3 + H(+M)$ (–R5), or by reaction between the initial reactants, $CH_4 + O_2 \rightarrow CH_3 + HO_2$ (–R13). The second subperiod is dominated by chain-branching processes. The methyl radical begins to react and slowly builds up a radical pool, which subsequently accelerates the fuel molecule destruction. The initiation phase takes only around 1% of the total ignition delay time, with the remainder occupied by fuel oxidation to intermediate products. Reactions in the postignition phase of the reaction, in which the intermediate species, such as CH_2O, CO, H_2, and C_2-hydrocarbons, are oxidized to products, are much faster than either the initiation or chain-branching periods in the ignition period. Owing to the rapidity, with which the final phase of the combustion takes place, different measures of the ignition delay period provide very similar results in the calculations [202].

The induction time obtained from the calculations is defined here to be the time at which the product of the oxygen atom and carbon monoxide concentrations is a maximum [201,202]. The agreement between measurements and predictions is very good at lean conditions, whereas at stoichiometric and rich conditions it is not better than a factor of 2. Beside the initiation steps (–R5, –R13), the most important reactions are the major chain-branching and chain-terminating steps. Chain branching proceeds primarily through the reactions $H + O_2 \rightarrow O + OH$, $CH_3 + O_2 \rightarrow CH_3O +$

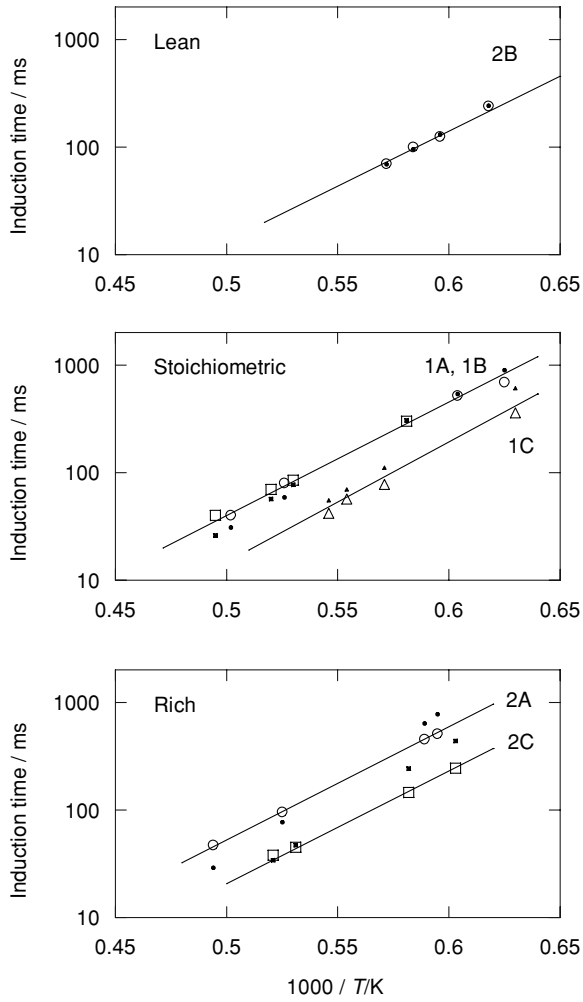

Figure A1 Comparison of measured [14] and predicted induction times for mixtures of CH_4 and O_2 in argon in a reflected wave shock tube for three stoichiometries: $\phi = 0.5$ (data set 2B), $\phi = 1.0$ (data sets 1A, 1B, and 1C), and $\phi = 2.0$ (data sets 2A and 2C). The open symbols denote data points, and the closed symbols are the corresponding calculated values. The lines represent the correlation obtained from the complete data of Lifshitz et al..

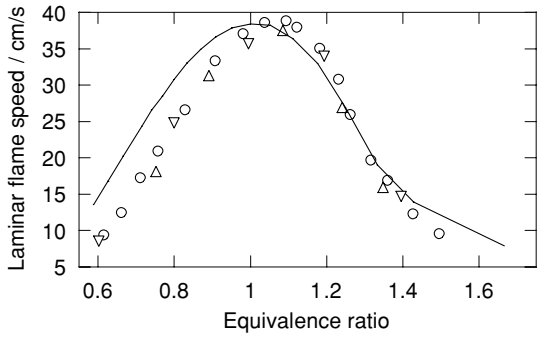

Figure A2 Comparison of measured and predicted laminar flame speeds for mixtures of CH_4 and air as function of fuel/air equivalence ratio. The open symbols denote experimental data (◯ [38], △ [39], ▽ [41]), and the line represents modeling predictions.

O (R10), $CH_3 + CH_3 \rightarrow C_2H_5 + H$ (R15), with both CH_3O and C_2H_5 dissociating rapidly to provide additional H-atoms (R42, –R112). Increasing the rate constants for these reactions will lead to shorter calculated ignition delay times. On the other hand, an increase in the rates of the major chain-terminating reactions will result in longer predicted induction times. The latter steps include $CH_4 + H \rightarrow CH_3 + H_2$ (R1), $CH_4 + OH \rightarrow CH_3 + H_2O$ (R3), and $CH_3 + CH_3(+M) \rightarrow C_2H_6(+M)$ (R14). Other important steps include reactions of CH_2O and HCO.

Results for laminar flame speeds have become important as validation data for kinetic models, in particular as the accuracy of these data has improved considerably over the last decade. The laminar flame speed depends on thermal and molecular diffusion properties, as well as the chemical reactivity of the reactants. Figure A2 compares measured [38,39,41] and predicted atmospheric pressure laminar flame speeds for mixtures of CH_4 and air as function of fuel/air equivalence ratio. The modeling predictions are seen to compare well with measurements under stoichiometric and rich conditions, whereas the burning rate is overpredicted under lean conditions.

Similarly to the ignition time delay calculations, predictions of the laminar flame speed are very sensitive to the major chain-branching and chain-terminating steps in the mechanism. Chain branching is dominated by the reactions $H + O_2 \rightarrow O + OH$, $CO + OH \rightarrow CO_2 + H$, $HCO(+M) \rightarrow CO + H(+M)$ (R85), and $CH_3 + OH \rightarrow {}^1CH_2 + H_2O$, whereas $H + O_2(+M) \rightarrow HO_2(+M)$, $CH_3 + H(+M) \rightarrow CH_4(+M)$ (R5), and $HCO + O_2 \rightarrow CO + HO_2$ (R91) are important for termination. Conceivably, the uncertainty in k_{91} at higher temperatures, as discussed above, contributes to the discrepancy at lean conditions. However, the choice of rate constants for a number of other reactions also influences the predicted flame speed.

The oxidation chemistry of methane and ethane in the 800–1500 K range at atmospheric pressure has previously been investigated under flow reactor conditions over a range of stoichiometries in our laboratory, e.g. [9,203]. Typical results obtained for CO in the outlet under lean and slightly fuel-rich conditions are shown in Fig. A3. The characteristic temperature regime for oxidation of the hydrocarbon to CO at the present reaction times differs significantly between the two fuels. Compared to methane, ethane is consumed at much lower temperatures at a given reaction time.

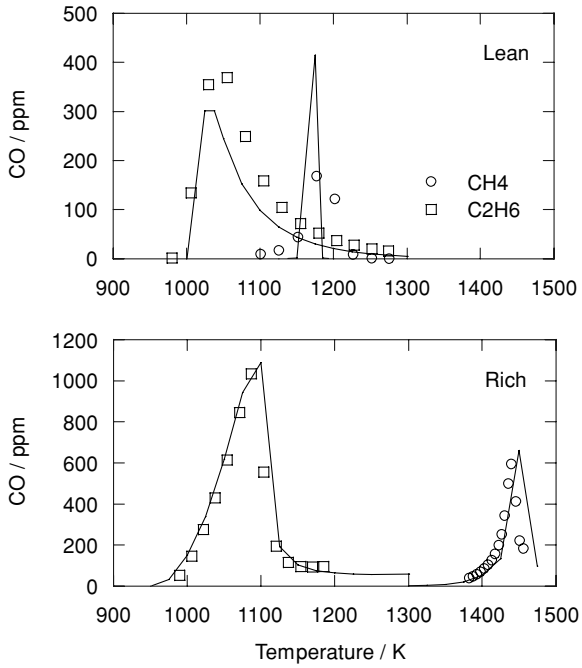

Figure A3 Comparison of measured and predicted CO exit concentrations from oxidation of CH_4 and C_2H_6 under diluted conditions in a flow reactor. The symbols denote experimental data, whereas the lines represent the modeling predictions. Lean sets: (a) $CH_4 = 2276$ ppm, $O_2 = 3.7\%$, $H_2O = 4.0\%$, balance N_2, $\tau = 249.6/T$ [9]; (b) $C_2H_6 = 237$ ppm, $O_2 = 4.0\%$, H_2O = trace, balance N_2, $\tau = 200/T$ [203]. Rich sets (P.G. Kristensen, P. Glarborg and K. Dam-Johansen, unpublished data): (a) $CH_4 = 1470$ ppm, $O_2 = 2685$ ppm, $H_2O = 1.9\%$, balance N_2, $\tau = 133.2/T$; (b) $C_2H_6 = 762$ ppm, $O_2 = 2437$ ppm, $H_2O = 1.8\%$, balance N_2, $\tau = 130.8/T$. In the modeling, a surface loss of CH_3OO corresponding to $k_{surf} = 10^5$ s^{-1} was assumed; this only affected predictions under lean conditions, shifting the initiation temperature to higher values.

This is consistent with shock tube ignition delay experiments reported in the literature [13].

The modeling predictions are in good agreement with the experimental data, in particular under slightly fuel-rich conditions. Similar to the high-pressure conditions reported earlier, there seem to be some sensitivity to surface loss of CH_3OO, but here only under lean conditions. Again the calculations, in particular the predicted onset of the reaction, are very sensitive to the formation and consumption of chain carriers. For methane, the most important steps to promote reaction are, in addition to initiation (–R5, –R13), $H + O_2 \rightarrow O + OH$, $CH_4 + OH \rightarrow CH_3 + H_2O$ (R3), $CH_3 + OH \rightarrow {}^1CH_2 + H_2O$, $CH_3 + O_2 \rightarrow CH_2O + OH$ (R11), and ${}^1CH_2 + O_2 \rightarrow CO + OH + H$. The most important terminating reactions are $HO_2 + OH \rightarrow H_2O + O_2$, $CH_3 + CH_3(+M) \rightarrow C_2H_6(+M)$ (R14), and ${}^1CH_2 + M \rightarrow CH_2 + M$. For ethane, the initiation occurs through $C_2H_6(+M) \rightarrow CH_3 + CH_3(+M)$ (–R14), while the radical pool is promoted by $H + O_2 \rightarrow O + OH$, $C_2H_6 + HO_2 \rightarrow C_2H_5 + H_2O_2$ (R97), $C_2H_5(+M) \rightarrow C_2H_4 + H(+M)$ (–R112), $H_2O_2(+M) \rightarrow OH + OH(+M)$, and limited primarily by $H + O_2(+M) \rightarrow HO_2(+M)$, $HO_2 + OH \rightarrow H_2O + O_2$, $C_2H_5 + O_2 \rightarrow C_2H_4 + HO_2$ (R107), and $C_2H_6 + H \rightarrow C_2H_5 + H_2$ (R94).

BIBLIOGRAPHY

1. Blundell, R. V.; Cook, W. G. A.; Hoare, D. E.; Milne, G. S. Proc Combust Inst 1965, 10, 445–452.
2. Vardanyan, I. A.; Nalbandyan, A. B. Int J Chem Kinet 1985, 17, 901–924.
3. Steinle, J. U.; Franck, E. U. Ber Bunsen-Ges Phys Chem 1995, 99, 66–73.
4. Williams, G. C.; Hottel, H. C.; Morgan, A. C. Proc Combust Inst 1965, 12, 913–925.
5. Rotzoll, G. Combust Sci Technol 1986, 47, 275–298.
6. Dagaut, P.; Boettner, J.-C.; Cathonnet, M. Combust Sci Technol 1991, 77, 127–148.
7. Hunter, T. B.; Wang, H.; Litzinger, T. A.; Frenklach, M. Combust Flame 1994, 97, 201–224.
8. Bromly, J. H.; Barnes, F. J.; Muris, S.; You, X.; Haynes, B. S. Combust Sci Technol 1996, 115, 259–296.
9. Bendtsen, A. B.; Glarborg, P.; Dam-Johansen, K. Combust Sci Technol 2000, 151, 31–71.
10. Skjøth-Rasmussen, M. S.; Glarborg, P.; Østberg, M.; Johannesen, J. T.; Livbjerg, H.; Jensen, A. D.; Christensen, T. S. Proc Combust Inst 2002, 29, 1329–1336.
11. Skjøth-Rasmussen, M. S.; Glarborg, P.; Østberg, M.; Johannessen, J. T.; Livbjerg, H.; Jensen, A. D.; Christensen, T. S. Combust Flame 2004, 136, 91–128.
12. Dagaut, P.; Nicolle, A. Combust Flame 2005, 140, 161–171.
13. Burcat, A.; Scheller, K.; Lifshitz, A. Combust Flame 1971, 16, 29–33.
14. Lifshitz, A.; Scheller, K.; Burcat, A.; Skinner, G. B. Combust Flame 1971, 16, 311–321.
15. Bowman, C. T. Proc Combust Inst 1974, 15, 869–882.
16. Dabora, E. K. Combust Flame 1975, 24, 181–184.
17. Olson, D. B.; Gardiner, W. C. Combust Flame 1978, 32, 151–161.
18. Roth, P.; Just, T. Proc Combust Inst 1984, 21, 807–818.
19. Spadaccini, L. J.; Colket, M. B. Prog Energy Combust Sci 1994, 20, 431–460.
20. Petersen, E. L.; Rohrig, M.; Davidson, D. F.; Hanson, R. K.; Bowman, C. T. Proc Combust Inst 1996, 26, 799–806.
21. Yang, H. X.; Qin, Z. W.; Lissianski, V. V.; Gardiner, W. C. Israel J Chem 1996, 36, 305–312.
22. Petersen, E. L.; Davidson, D. F.; Hanson, R. K. Combust Flame 1999, 117, 272–290.

23. Zhukov, V. P.; Sechenov, V. A.; Starikovskii, A. Y. Combust Explosion Shock Waves 2003, 39, 487–495.
24. Huang, J.; Hill, P. G.; Bushe, W. K.; Munshi, S. R. Combust Flame 2004, 136, 25–42.
25. Levy, Y.; Olchanski, E.; Sherbaurn, V.; Erenburg, V.; Burcat, A. J Propulsion Power 2006, 22, 669–676.
26. Peeters, J.; Mahnen, G. Proc Combust Inst 1974, 14, 133–146.
27. Peeters, J.; Vinckier, C. Proc Combust Inst 1974, 15, 969–976.
28. Bechtel, J. H.; Blint, R. J.; Dasch, C. J.; Weinberger, D. A. Combust Flame 1981, 42, 197–213.
29. Langley, C. J.; Burgess, A. R. Proc R Soc London A 1989, 421, 259–278.
30. Hennessy, R. J.; Robinson, C.; Smith, D. B. Proc Combust Inst 1986, 21, 761–772.
31. Rothschild, W. G.; Kaiser, E. W.; Lavoie, G. A. Combust Sci Technol 1986, 140, 209–227.
32. Egolfopoulos, F. N.; Cho, P.; Law, C. K. Combust Flame 1989, 76, 375–391.
33. Heard, D. E.; Jeffries, J. B.; Smith, G. P.; Crosley, D. R. Combust Flame 1992, 88, 137–148.
34. Vandooren, J.; van Tiggelen, P. J. Combust Flame 1992, 90, 247–258.
35. Castaldi, J.; Vincitore, A. M.; Senkan, S. M. Combust Sci Technol 1995, 107, 1–19.
36. Williams, B. A.; Fleming, J. W. Combust Flame 1995, 100, 571–590.
37. Musick, M.; van Tiggelen, P. J.; Vandooren, J. Combust Flame 1996, 105, 433–450.
38. Davies, S. G.; Law, C. K. Combust Sci Technol 1998, 140, 427–449.
39. Vagepoulos, C. M.; Egolfopoulos, F. N. Proc Combust Inst 1998, 27, 1341–1347.
40. Berg, P. A.; Hill, D. A.; Noble, A. R.; Smith, G. P.; Jeffries, J. B.; Crosley, D. R. Combust Flame 2000, 121, 223–235.
41. Dong, Y.; Vagepoulos, C. M.; Spedding, G. R.; Egolfopoulos, F. N. Proc Combust Inst 2002, 29, 1419–1426.
42. Turbiez, A.; Bakali, A. E.; Pauwels, J. F.; Rida, A.; Meunier, P. Fuel 2004, 83, 933–941.
43. Newitt, D. M.; Haffner, A. E. Proc R Soc London Ser A 1932, 125, 277–291.
44. Yarlagadda, P. S.; Morton, L. A.; Hunter, N. R.; Gesser, H. D. Ind Eng Chem Res 1988, 27, 252–256.
45. Burch, R.; Squire, G. D.; Tsang, S. C. J Chem Soc Faraday Trans 1 1989, 85, 3561–3568.
46. Hunter, N. R.; Gesser, H. D.; Morton, L. A.; Yarlagadda, P. S. Appl Catal 1990, 57, 45–54.
47. Thomas, D. J.; Willi, R.; Baiker, A. Ind Eng Chem Res 1992, 31, 2272–2278.
48. Chun, J.-W.; Anthony, R. G. Ind Eng Chem Res 1993, 32, 259–263.
49. Casey, P. S.; McAllister, T.; Foger, K. Ind Eng Chem Res 1994, 33, 1120–1125.
50. Feng, W.; Knopf, F. C.; Dooley, K. M. Energy Fuels 1994, 8, 815–822.
51. Chellappa, A. S.; Fuangfoo, S.; Viswanath, D. S. Ind Eng Chem Res 1997, 36, 1401–1409.
52. Zhang, Q.; He, D.; Li, J.; Xu, B.; Liang, Y.; Zhu, Q. Appl Catal A: Gen 2002, 224, 201–207.
53. Webley, P. A.; Tester, J. W. Energy Fuels 1991, 5, 411–419.
54. Savage, P. E.; Li, R. K.; Santini, J. T. J Supercrit Fluids 1994, 7, 135–144.
55. Lee, J. H.; Foster, N. R. J Supercrit Fluids 1996, 9, 99–105.
56. Steeper, R. R.; Rice, S. F.; Kennedy, I. M.; Aiken, J. D. J Phys Chem 1996, 100, 184–189.
57. Savage, P. E.; Yu, J. L.; Stylski, N.; Brock, E. E. J Supercrit Fluids 1998, 12, 141–153.
58. Sato, T.; Watanabe, M.; Smith, R. L.; Adschiri, T.; Arai, K. J Supercrit Fluids 2004, 28, 69–77.
59. Rasmussen, C. L.; Hansen, J.; Marshall, P.; Glarborg, P. Int J Chem Kinet, in press.
60. Levenspiel, O. Chemical Reaction Engineering, 2nd ed.; Wiley: New York, 1972.
61. Levenspiel, O. The Chemical Reactor Omnibook; OSU Book Stores, Inc.: Corvallis, OR, 1993.
62. Rasmussen, C. L.; Andersen, K. H.; Dam-Johansen, K.; Glarborg, P. Int J Chem Kinet, in press.
63. Burcat, A.; Ruscic, B. Report TAE960, Technion Israel Institute of Technology, September 16, 2005.
64. Ruscic, B.; Pinzon, R. E.; Morton, M. L.; von Laszevski, G.; Bittner, S. J.; Nijsure, S. G.; Amin, K. A.; Minkoff, M.; Wagner, A. F. J Phys Chem A 2004, 108, 9979–9997.
65. Ruscic, B.; Pinzon, R. E.; Morton, M. L.; Srinivasan, N. K.; Su, M.-C.; Sutherland, J. W.; Michael, J. V. J Phys Chem A 2006, 110, 6592–6601.
66. Matthews, J.; Sinha, A.; Francisco, J. S. J Chem Phys 2005, 122, 221101.
67. Blanksby, S. J.; Ramond, T. M.; Davico, G. E.; Nimlos, M. R.; Kato, S.; Bierbaum, V. M.; Lineberger, W. C.; Ellison, G. B.; Okumura, M. J Am Chem Soc 2001, 123, 9585–9596.
68. Janoschek, R.; Rossi, M. J. Int J Chem Kinet 2002, 34, 550–560.
69. Knyazev, V. D.; Slagle, I. R. J Phys Chem A 1998, 102, 1770–1778.
70. Meloni, G.; Zou, P.; Klippenstein, S. J.; Ahmed, M.; Leone, S. R.; Taatjes, C. A.; Osborn, D. L. J Am Chem Soc 2006, 128, 13559–13567.
71. Jungkamp, T. P. W.; Seinfeld, J. H. Chem Phys Lett 1996, 257, 15–22.
72. Lay, T. H.; Bozzelli, J. W. J Phys Chem A 1997, 101, 9505–9510.
73. Carstensen, H.-H.; Dean, A. M. Proc Combust Inst 2005, 30, 995–1003.
74. Sutherland, J. W.; Su, M. C.; Michael, J. V. Int J Chem Kinet 2001, 33, 669–684.
75. Srinivasan, N. K.; Su, M.-C.; Sutherland, J. W.; Michael, J. V. J Chem Phys A 2005, 109, 1857–1863.
76. Baulch, D. L.; Bowman, C. T.; Cobos, C. J.; Cox, R. A.; Just, T.; Kerr, J. A.; Pilling, M. J.; Stocker, D.;

Troe, J.; Tsang, W.; Walker, R. W.; Warnatz, J. J Phys Chem Ref Data 2005, 34, 757–1397.
77. Baldwin, R. R.; Jones, P. N.; Walker, R. W. J Chem Soc, Faraday Trans 2 1988, 84, 199–207.
78. Zhu, R. S.; Lin, M. C. J Chem Phys A 2001, 105, 6243–6248.
79. Scire, J. J. Jr.; Yetter, R. A.; Dryer, F. L. Int J Chem Kinet 2001, 33, 75–100.
80. Srinivasan, N. K.; Michael, J. V.; Harding, L. B.; Klippenstein, S. J. Combust Flame 2007, 149, 104–111.
81. Fernandes, R. X.; Luther, K.; Troe, J. J Phys Chem A 2006, 110, 4442–4449.
82. Kee, R. J.; Rupley, F. M.; Miller, J. A. Sandia Report SAND89–8009B•UC–706, Sandia National Laboratories, Livermore, CA, 1989.
83. Srinivasan, N. K.; Su, M.-C.; Sutherland, J. W.; Michael, J. V. J Chem Phys A 2005, 109, 7902–7914.
84. Yu, C.-L.; Wang, C.; Frenklach, M. J Phys Chem 1995, 99, 14377–14387.
85. Hwang, S. M.; Ryu, S.-O.; De Witt, K. J.; Rabinowitz, M. J. J Phys Chem A 1999, 103, 5949–5958.
86. Herbon, J. T.; Hanson, R. K.; Bowman, C. T.; Golden, D. M. Proc Combust Inst 2005, 30, 955–963.
87. Colket, III, M. B.; Naegeli, D. W.; Glassman, I. Proc Combust Inst 1977, 16, 1023–1039.
88. Reid, I. A. B.; Robinson, C.; Smith, D. B. Proc Combust Inst 1984, 20, 1833–1843.
89. Cobos, C. J.; Troe, J. Z Phys Chem N F 1990, 167, 129–149.
90. Hwang, S. M.; Wagner, H. G.; Wolff, T. Proc Combust Inst 1990, 23, 99–105.
91. Hwang, S. M.; Rabinowitz, M. J.; Gardiner, W. C., Jr.; Chem Phys Lett 1993, 205, 157–162.
92. Du, H.; Hessler, J. P.; Ogren, P. J. J Phys Chem 1996, 100, 974–983.
93. Pesa, M.; Pilling, M. J.; Robertson, S. H.; Wardlaw, D. M. J Phys Chem A 1998, 102, 8526–8536.
94. Pacey, P. D. J Phys Chem A 1998, 102, 8541–8547.
95. Glänzer, K.; Quack, M.; Troe, J. Chem Phys Lett 1976, 39, 304–309.
96. Glänzer, K.; Quack, M.; Troe, J. Proc Combust Inst 1977, 16, 949–960.
97. Hessler, J. P.; Ogren, P. J. J Phys Chem 1996, 100, 984–992.
98. Seakins, P. W.; Leone, S. R. J Phys Chem 1992, 96, 4478–4485.
99. Marcy, T. P.; Díaz, R. R.; Heard, D.; Leone, S. R.; Harding, L. B.; Klippenstein, S. J. J Phys Chem A 2001, 105, 8361–8369.
100. Preses, J. M.; Fockenberg, C.; Flynn, G. W. J Phys Chem A 2000, 104, 6758–6763.
101. De Avillez Pereira, R.; Baulch, D. L.; Pilling, M. J.; Robertson, S. H.; Zeng, G. J Phys Chem A 1997, 101, 9681–9693.
102. Wilson, C.; Balint-Kurti, G. G. J Phys Chem A 1998, 102, 1625–1631.
103. Dean, A. M.; Westmoreland, P. R. Int J Chem Kinet 1987, 19, 207–228.
104. Humpfer, R.; Oser, H.; Grotheer, H.-H.; Just, T. Proc Combust Inst 1994, 25, 721–731.
105. Deters, R.; Otting, M.; Wagner, H. G.; Temps, F.; Laszlo, B.; Dobe, S.; Berces, T. Ber Bunsen-Ges Phys Chem 1998, 102, 58–72.
106. Tsang, W.; Hampson, R. J Phys Chem Ref Data 1986, 15, 1087–1279.
107. Watt, J. D.; Francisco, J. S. J Chem Phys 2006, 125, 104301.
108. Tyndall, G. S.; Cox, R. A.; Granier, C.; Lesclaux, R.; Moortgat, G. K.; Pilling, M. J.; Ravishankara, A. R.; Wallington, T. J. J Geophys Res 2001, 106, 12157–12182.
109. Wallington, T. J.; Japar, S. M. Chem Phys Lett 1990, 167, 513–518.
110. Wallington, T. J. J Chem Soc, Faraday Trans 1991, 87, 2379–2382.
111. Elrod, M. J.; Ranschaert, D. L.; Schneider, N. J. Int J Chem Kinet 2001, 33, 363–376.
112. Keiffer, M.; Pilling, M. J.; Smith, M. J. C. J Phys Chem 1987, 91, 6028–6034.
113. Keiffer, M.; Miscampbell, A. J.; Pilling, M. J. J Chem Soc, Faraday Trans 2 1988, 84, 505–514.
114. Park, D. A. Int J Chem Kinet 1977, 9, 451–469.
115. Pilling, M. J.; Smith, M. J. C. J Phys Chem 1985, 89, 4713–4720.
116. Kirk, A. D. Can J Chem 1965, 43, 2236–2242.
117. Lightfoot, P. D.; Roussel, P.; Caralp, F.; Lesclaux, R. J Chem Soc, Faraday Trans 1991, 87, 3213–3220.
118. Hippler, H.; Striebel, F.; Viskolcz, B. Phys Chem Chem Phys 2001, 3, 2450–2458.
119. Wantuck, P. J.; Oldenborg, R. C.; Baughcum, S. L.; Winn, K. R. Proc Combust Inst 1988, 22, 973–981.
120. Shaw, R.; Thynne, J. C. J Trans Faraday Soc 1966, 62, 104–111.
121. Eiteneer, B.; Yu, C.-L.; Goldenberg, M.; Frenklach, M. J Phys Chem A 1998, 102, 5196–5205.
122. Vasudevan, V.; Davidson, D. F.; Hanson, R. K. Int J Chem Kinet 2005, 37, 98–109.
123. Sivakumaran, V.; Hölscher, D.; Dillon, T. J.; Crowley, J. N. Phys Chem Chem Phys 2003, 5, 4821–4827.
124. Vasudevan, V.; Davidson, D. F.; Hanson, R. K.; Bowman, C. T.; Golden, D. M. Proc Combust Inst 2007, 31, 175–183.
125. Hippler, H.; Krasteva, N.; Striebel, F. Phys Chem Chem Phys 2004, 6, 3383–3388.
126. Hippler, H.; Krasteva, N.; Striebel, F. Phys Chem Chem Phys 2005, 7, 2077–2079.
127. DeSain, J. D.; Jusinski, L. E.; Ho, A. D.; Taatjes, C. A. Chem Phys Lett 2001, 347, 79–86.
128. Colberg, M.; Friedrichs, G. J Phys Chem A 2006, 110, 160–170.
129. Mahmud, K.; Marshall, P.; Fontijn, A. J Chem Phys 1988, 88, 2393–2397.
130. Braun, W.; Lenzi, M. Discuss Faraday Soc 1967, 44, 252.
131. Clarke, J. S.; Donahue, N. M.; Kroll, J. H.; Rypkema, H. A.; Anderson, J. G. J Chem Phys A 2000, 104, 5254–5264.

132. Miller, J. A.; Klippenstein, S. J.; Robertson, S. R. Proc Combust Inst 2000, 28, 1479–1486.
133. Miller, J. A.; Klippenstein, S. J. Int J Chem Kinet 2001, 33, 654–668.
134. Ludwig, W.; Brandt, B.; Friedrichs, G.; Temps, F. J Phys Chem A 2006, 110, 3330–3337.
135. Dobis, O.; Benson, S. W. J Am Chem Soc 1993, 115, 8798–8809.
136. Smith, G. P.; Golden, D. M.; Frenklach, M.; Moriarty, N. W.; Eiteneer, B.; Goldenberg, M.; Bowman, C. T.; Hanson, R. K.; Song, S.; Gardiner, W. C., Jr.; Lissianski, V. V.; Qin, Z. "GRI-Mech 3.0 Database," Gas Research Institute, 2000.
137. Harding, L. B.; Klippenstein, S. J. Proc Combust Inst 1998, 27, 151–157.
138. Slagle, I. R.; Sarzynski, D.; Gutman, D.; Miller, J. A.; Melius, C. F. J Chem Soc, Faraday Trans 2 1988, 84, 491–503.
139. Hoyermann, K.; Olzmann, M.; Seeba, J.; Viskolcz, B. J Phys Chem A 1999, 103, 5692–5698.
140. Lindner, J.; Loomis, R. A.; Klaassen, J. J.; Leone, S. R. J Chem Phys 1998, 108, 1944–1952.
141. Reid, J. P.; Marcy, T. P.; Kuehn, S.; Leone, S. R. J Chem Phys 2000, 113, 4572–4580.
142. Fagerström, K.; Lund, A.; Mahmoud, G.; Jodkowski, J. T.; Ratajczak, E. Chem Phys Lett 1993, 208, 321–327.
143. Marinov, N. M. Int J Chem Kinet 1999, 31, 183–220.
144. Kirk, A. D.; Knox, J. H. Trans Faraday Soc 1960, 56, 1296–1303.
145. Cattell, F. C.; Cavanagh, J.; Cox, R. A.; Jenkin, M. E. J Chem Soc, Faraday Trans 2 1986, 82, 1999–2018.
146. Dagaut, P.; Wallington, T. J.; Kurylo, M. J. J Phys Chem 1988, 92, 3836–3839.
147. Fenter, F. F.; Catoire, V.; Lesclaux, R.; Lightfoot, P. D. J Phys Chem 1993, 97, 3530–3538.
148. Maricq, M. M.; Szente, J. J. J Phys Chem 1994, 98, 2078–2082.
149. Boyd, A. A.; Flaud, P.-M.; Daugey, N.; Lesclaux, R. J Phys Chem A 2003, 107, 818–821.
150. Wallington, T. J.; Japar, S. M. Chem Phys Lett 1990, 166, 495–499.
151. Spittler, M.; Barnes, I.; Becker, K. H.; Wallington, T. J. Chem Phys Lett 2000, 321, 57–61.
152. Hasson, A. S.; Tyndall, G. S.; Orlando, J. J. J Phys Chem A 2004, 108, 5979–5989.
153. Hou, H.; Li, J.; Song, X.; Wang, B. J Phys Chem A 2005, 109, 11206–11212.
154. Adachi, H.; Basco, N.; James, D. G. L. Int J Chem Kinet 1979, 11, 1211–1229.
155. Niki, H.; Maker, P. D.; Savage, C. M.; Breitenbach, L. P. J Phys Chem 1982, 86, 3825–3829.
156. Anastasi, C.; Waddington, D. J.; Woolley, A. J Chem Soc, Faraday Trans 1 1983, 79, 505–516.
157. Munk, J.; Pagsberg, P.; Ratajczak, E.; Sillesen, A. J Phys Chem 1986, 90, 2752–2757.
158. Wallington, T. J.; Dagaut, P.; Kurylo, M. J. J Photochem Photobiol A: Chem 1988, 19, 173–185.
159. Wallington, T. J.; Gierczak, C. A.; Ball, J. C.; Japar, S. M. Int J Chem Kinet 1989, 21, 1077–1089.
160. Bauer, D.; Crowley, J. N.; Moortgat, G. K. J Photochem Photobiol A: Chem 1992, 65, 329–344.
161. Atkinson, D. B.; Hudgens, J. W. J Phys Chem A 1997, 101, 3901–3909.
162. Lightfoot, P. D.; Cox, R. A.; Crowley, J. N.; Destriau, M.; Hayman, G. D.; Jenkin, M. E.; Moortgat, G. K.; Zabel, F. Atmos Environ A 1992, 26, 1805–1961.
163. Somnitz, H.; Zellner, R. Phys Chem Chem Phys 2000, 2, 1899–1905.
164. Somnitz, H.; Zellner, R. Phys Chem Chem Phys 2000, 2, 1907–1918.
165. Caralp, F.; Devolder, P.; Fittschen, C.; Gomez, N.; Hippler, H.; Méreau, R.; Rayez, M. T.; Striebel, F.; Viskolcz, B. Phys Chem Chem Phys 1999, 1, 2935–2944.
166. Rauk, A.; Boyd, R. J.; Boyd, S. L.; Henry, D. J.; Radom, L. Can J Chem 2003, 81, 431–442.
167. Zhang, Y.; Zhang, S.; Li, Q. S. Chem Phys 2004, 296, 79–86.
168. Atkinson, R. J Phys Chem Ref Data 1997, 26, 215–290.
169. Orlando, J. J.; Tyndall, G. S.; Wallington, T. J. Chem Rev 2003, 103, 4657–4689.
170. Curran, H. J. Int J Chem Kinet 2006, 38, 250–275.
171. Batt, L. Int J Chem Kinet 1979, 11, 977–993.
172. Gutman, D.; Sanders, N.; Butler, J. E. J Phys Chem 1982, 86, 66–70.
173. Hartmann, D.; Karthauser, J.; Sawerysyn, J. P.; Zellner, R. Ber Bunsen-Ges Phys Chem 1990, 94, 639–645.
174. Fittschen, C.; Frenzel, A.; Imrik, K.; Devolder, P. Int J Chem Kinet 1999, 31, 860–866.
175. Zabarnick, S.; Heicklen, J. Int J Chem Kinet 1985, 17, 455–476.
176. Setokuchi, O.; Sato, M. J Phys Chem A 2002, 106, 8124–8132.
177. Zhu, R. S.; Park, J.; Lin, M. C. Chem Phys Lett 2005, 408, 25–30.
178. Atkinson, R.; Perry, R. A.; Pitts, J. N., Jr.; J Chem Phys 1977, 66, 1197–1201.
179. Liu, A.; Mulac, W. A.; Jonah, C. D. J Chem Phys 1988, 92, 3828–3833.
180. Diau, E. W.-G.; Lee, Y.-P. J Chem Phys 1992, 96, 377.
181. Klemm, R. B.; Sutherland, J. W.; Wickramaaratchi, M. A.; Yarwood, G. J Phys Chem 1990, 94, 3354–3357.
182. Hunziker, H. E.; Kneppe, H.; Wendt, H. R. J Photochem 1981, 17, 377–387.
183. Smalley, J. F.; Nesbitt, F. L.; Klemm, R. B. J Phys Chem 1986, 90, 491–497.
184. Koda, S.; Endo, Y.; Hirota, E.; Tsuchiya, S. J Phys Chem 1987, 91, 5840–5842.
185. Schmoltner, A. M.; Chu, P. M.; Brudzynski, R. J.; Lee, Y. T. J Chem Phys 1989, 91, 6926–6936.
186. Koda, S.; Endo, Y.; Tsuchiya, S.; Hirota, E. J Phys Chem 1991, 95, 1241–1244.
187. Anastasi, C.; Sanderson, M. G.; Pagsberg, P.; Sillesen, A. J Chem Soc, Faraday Trans 1994, 90, 3625–3631.

188. Baldwin, R. R.; Stout, D. R.; Walker, R. W. J Chem Soc, Faraday Trans 1 1984, 80, 3481–3489.
189. Baldwin, R. R.; Dean, C. E.; Walker, R. W. J Chem Soc, Faraday Trans 2 1986, 82, 1445–1455.
190. Baldwin, R. R.; Stout, D. R.; Walker, R. W. J Chem Soc, Faraday Trans 1991, 87, 2147–2150.
191. Ignatyev, I. S.; Xie, Y.; Allen, W. D.; Schaefer, H. F., III. J Chem Phys 1997, 107, 141–155.
192. Rienstra-Kiracofe, J. C.; Allen, W. D.; Schaefer, H. F., III. J Phys Chem A 2000, 104, 9823–9840.
193. Benson, S. W. Int J Chem Kinet 1996, 28, 665–672.
194. Ervin, K. M.; DeTuri, V. F. J Phys Chem A 2002, 106, 9947–9956.
195. Lutz, A. E.; Kee, R. J.; Miller, J. A. Sandia Report SAND87–8248•UC–401, Sandia National Laboratories, Livermore, CA, 1990.
196. Rytz, D. W.; Baiker, A. Ind Eng Chem Res 1991, 30, 2287–2292.
197. Ozturk, S.; Onal, I.; Senkan, S. Ind Eng Chem Res 2000, 39, 250–258.
198. Vedeneev, V. I.; Arutyunov, V. S.; Krymov, N. Y.; Cherbakov, P. M.; Sedykh, A. D. Catal Today 1992, 13, 613–616.
199. Senosiain, J. P.; Klippenstein, S. J.; Miller, J. A. J Phys Chem A 2007, 110, 6960–6970.
200. Glarborg, P.; Alzueta, M. U.; Dam-Johansen, K.; Miller, J. A. Combust Flame 1998, 115, 1–27.
201. Sloane, T. M. Combust Sci Technol 1989, 63, 287.
202. Westbrook, C. K. Combust Sci Technol 1979, 20, 5.
203. Hjuler, K.; Glarborg, P.; Dam-Johansen, K. Ind Eng Chem Res 1995, 34, 1882–1888.
204. Janoschek, R.; Rossi, M. J. Int J Chem Kinet 2004, 36, 661–686.
205. You, X.; Wang, H.; Goos, E.; Sung, C.-J.; Klippenstein, S. J. J Chem Phys A 2007, 111, 4031–4042.
206. Slemr, F.; Warneck, P. Int J Chem Kinet 1977, 9, 267–282.
207. Vaghjiani, G. L.; Ravishankara, A. R. J Phys Chem 1989, 93, 1948–1959.
208. Ing, W.-C.; Sheng, C. Y.; Bozzelli, J. W. Fuel Proc Technol 2003, 83, 111–145.
209. Dóbé, S.; Bérces, T.; Szilagyi, I. J Chem Soc, Faraday Trans 1991, 87, 2331–2336.
210. Ewig, F.; Rhäsa, D.; Zellner, R. Ber Bunsen-Ges Phys Chem 1987, 91, 708–717.
211. Wantuck, P. J.; Oldenborg, R. C.; Baughcum, S. L.; Winn, K. R. J Chem Phys 1987, 91, 4653–4655.
212. Wang, B.; Hou, H.; Gu, Y. J Chem Phys A 1999, 103, 8021–8029.
213. Held, T. J.; Dryer, F. L. Int J Chem Kinet 1998, 30, 805–830.
214. Seetula, J. A.; Kalinovski, I. J.; Slagle, I. R.; Gutman, D. Chem Phys Lett 1994, 224, 533–538.
215. Tsang, W. J Phys Chem Ref Data 1987, 16, 471–508.
216. Friedrichs, G.; Herbon, J. T.; Davidson, D. F.; Hanson, R. K. Int J Chem Kinet 2004, 36, 157–169.
217. Troe, J. J Phys Chem A 2005, 109, 8320–8328.
218. Friedrichs, G.; Herbon, J. T.; Davidson, D. F.; Hanson, R. K. Phys Chem Chem Phys 2002, 4, 5778–5788.
219. Callear, A. B.; Cooper, I. A. Chem Phys Lett 1989, 155, 146–152.
220. Stewart, P. H.; Rothem, T.; Golden, D. M. Proc Combust Inst 1988, 22, 943–952.
221. Baggott, J. E.; Frey, H. M.; Lightfoot, P. D.; Walsh, R. J Phys Chem 1987, 91, 3386–3393.
222. Harding, L. B.; Georgievskii, Y.; Klippenstein, S. J. J Phys Chem A 2005, 109, 4646–4656.
223. Monks, P. S.; Nesbitt, F. L.; Payne, W. A.; Scanlon, M.; Stief, L. J.; Shallcross, D. E. J Phys Chem 1995, 99, 17151–17159.
224. Miller, J. A.; Melius, C. F. Combust Flame 1992, 91, 21–39.
225. Fahr, A.; Laufer, A. H.; Klein, R.; Braun, W. J Phys Chem 1991, 95, 3218–3224.
226. Gupte, K. S.; Kiefer, J. H.; Tranter, R. S.; Klippenstein, S. J.; Harding, L. B. Proc Combust Inst 2006, 31, 167–174.
227. Baulch, D. L.; Cobos, C. J.; Cox, R. A.; Esser, C.; Frank, P.; Just, T.; Kerr, J. A.; Pilling, M. J.; Troe, J.; Walker, R. W.; Warnatz, J. J Phys Chem Ref Data 1992, 21, 411–734.
228. Taylor, P. H.; Rahman, M. S.; Arif, M.; Dellinger, B.; Marshall, P. Proc Combust Inst 1996, 26, 497.
229. Cameron, M.; Sivakumaran, V.; Dillon, T. J.; Crowley, J. N. Phys Chem Chem Phys 2002, 4, 3628–3638.
230. Senosiain, J. P.; Klippenstein, S. J.; Miller, J. A. J Phys Chem A 2006, 110, 5772–5781.
231. Ohmori, K.; Miyoshi, A.; Matsui, H.; Washida, N. J Phys Chem 1990, 94, 3253–3255.
232. Bartels, M.; Edelbüttel-Einhaus, J.; Hoyermann, K. Proc Combust Inst 1991, 23, 131–138.
233. Adachi, H.; Basco, N.; James, D. G. L. Int J Chem Kinet 1981, 13, 1251–1276.
234. Tyndall, G. S.; Orlando, J. J.; Wallington, T. J.; Hurley, M. D. Int J Chem Kinet 1997, 29, 655–663.
235. Marinov, N. M.; Pitz, W. J.; Westbrook, C. K.; Castaldi, M. J.; Senkan, S. M. Combust Sci Technol 1996, 116, 211–287.
236. Hranisavljevic, J.; Kumaran, S. S.; Michael, J. V. Proc Combust Inst 1998, 27, 159–166.
237. Grussdorf, J.; Nolte, J.; Temps, F.; Wagner, H. G. Ber Bunsen-Ges Phys Chem 1994, 98, 546–553.